# Rapid shear of initially anisotropic turbulence in a rotating frame

E. Akylas,[a] S. C. Kassinos,[b] and C. A. Langer
*Department of Mechanical and Manufacturing Engineering, University of Cyprus, Nicosia 1678, Cyprus*

(Received 8 September 2006; accepted 15 January 2007; published online 27 February 2007)

In the present study, we investigate, using inviscid rapid distortion theory, the evolution of sheared turbulence in a rotating frame as a function of the rotation rate (including stable, transitional, and unstable regimes), and examine the sensitivity of the results for various nonisotropic initial conditions. Analytical solutions are derived for the evolution of the stresses and the structure dimensionality tensor components for three one-dimensional and three two-dimensional initializations. From these solutions, we calculate the asymptotic states of the turbulence, which are compared to the exact numerical solution of the three-dimensional initially isotropic case. From the investigation it is shown that the qualitative characteristics of the isotropic solution in the unstable regime are represented quite accurately when the initial turbulence is dependent at least on the axis of the rotation of the frame. For the transitional and the stable regimes, though, the initial dependence of the turbulence on the axis of the mean flow is also crucial. © *2007 American Institute of Physics*. [DOI: 10.1063/1.2675939]

## I. INTRODUCTION

The effects of system rotation on turbulent shear flows have received considerable attention because of their relevance to important technological and astrophysical problems. The state of sheared turbulence changes significantly when it is subjected to frame rotation. Numerical studies (Bardina *et al.*,[1] Lee *et al.*,[2] Salhi and Cambon[3]) have clearly shown that rotation can act to either stabilize or destabilize turbulent shear flow, depending on the ratio of the frame rotation rate to the shear rate. Recently, Brethouwer[4] has used a combination of theoretical analysis and numerical simulations to investigate the effect of frame rotation on the transport of a passive scalar in homogeneous shear flow. Studies such as these have helped to clarify the global features of homogeneous shear flow in a rotating frame.

Apart from experiments and direct numerical simulations (DNS), considerable insight in the stability of rotated shear flows can be gained through rapid distortion theory (RDT). In the framework of RDT, linearized equations of motion are used to explain some of the significant kinematical and dynamical responses of turbulence to imposed deformation. The theory is valid for all kinds of rapidly changing turbulent flows, when the distortion is applied for a time that is short compared to the "turn-over" time scale of the energy containing eddies; that is, the initial response to a sudden change in the mean deformation. Furthermore, RDT is also a good approximation, in cases where the ratio of the mean deformation time scale over the eddy turn-over time scale is much smaller than 1 (Pope,[5] Hanazaki and Hunt[6]), which ensures that the nonlinear terms in the governing turbulence equations involving products of fluctuation quantities are still negligible; then the turbulence is affected mostly by the mean flow and not by the turbulence itself. Thus, the nonlinear terms are neglected, resulting in RDT equations that are linear in the fluctuation quantities. The solutions to these linearized equations can be used to calculate the characteristics of the development of the energy spectrum tensor, two-point correlations and other turbulence statistical quantities of interest. For example, in the case of homogeneous shear in a rotating frame, a comparison of the values of the normalized Reynolds stress components predicted by inviscid RDT at $St=10$ with the corresponding values predicted by the large-eddy simulation (LES) of Bardina *et al.*, shows the two to be in excellent agreement (Kassinos and Reynolds[7]). Although RDT equations imply simplifications, for many cases they can be considered valid. In real nature there are regions of turbulent flows, far from equilibrium, where the local production of turbulent kinetic energy outweighs dissipation, and where the turbulence time scale is substantially larger than the mean flow time scale. For instance, in the viscous near-wall region of the ubiquitous turbulent boundary layer, the ratio of the above time scales is of the order of 10 and RDT can give useful insight. More specifically, fully nonlinear DNS results (Spalart,[8] Moser[9]) point to a distribution of energy in the Reynolds stress tensor, significantly different from the log-layer distribution, and in fact, though still far, it does grow impressively close to the asymptotic shear limits predicted from RDT. In addition, when a given flow suddenly encounters a new type of mean deformation, shear, or rotation, the initial response of the turbulence is well described by RDT, as in the case of flow over obstacles (Britter *et al.*,[10] Gong *et al.*[11]). In general, the investigation of RDT solutions offers qualitative information for the trends of the turbulent structure in real problems, as, for example, the investigation of the stably stratified boundary layer (Galmiche and Hunt[12]) and the nonstratified log-layer (Nazarenko[13]).

RDT is a closed theory for two-point correlations or spectra, but the one-point governing equations are, in general, not closed due to the nonlocality of the pressure fluc-

[a]Also with the Institute of Environmental Research, National Observatory of Athens, Greece.
[b]Also with the Center for Turbulence Research, Stanford University/NASA-Ames. Electronic mail: kassinos@ucy.ac.cy

 

tuations (Townsend,[14] Hunt,[15] Savill,[16] Hunt and Carruthers,[17] Cambon and Scott[18]). Simple cases of rapid deformation often admit closed-form solutions for individual Fourier coefficients. Even when such closed-form solutions are possible in spectral space, the integrals involved in forming the corresponding one-point statistics are often too complex to evaluate in closed form, and one is then forced to resort to numerical integration. The few cases for which closed-form solutions can be obtained for one-point statistics, like the Reynolds stresses, offer valuable insight. For example, Salhi[19] derived complicated analytical expressions for the evolution of the turbulent kinetic energy spectrum for generalized frame rotation rates. Rogers[20] was able to find closed-form solutions for all the components of the spectrum tensor for homogeneous turbulence that is being sheared in a fixed frame. These solutions provide valuable insight in the distribution of energy in spectral space and also lead to some estimates of the asymptotic behavior of one-point statistics, such as the Reynolds stresses, in the limit of large total shear. Akylas *et al.*[21] have looked at the case of homogeneous turbulence that is sheared in a frame that counter-rotates at a rotation rate that matches in magnitude the rotation associated with the mean shear. Along with spectral solutions, they have also derived analytical expressions for the evolution of the stresses and the structure dimensionality tensor components in physical space.

In the present study we use inviscid RDT to investigate the evolution of turbulence for various rotation rates, examining the sensitivity of the solutions to various nonisotropic initial conditions. The investigation covers the development of the Reynolds stresses $R_{ij}=\overline{u_i u_j}$ and the structure dimensionality tensor $D_{ij}$, introduced by Kassinos *et al.*[22] (see Sec. III). The combined use of these tensors allows one to distinguish between the componentality of the turbulence (described by the Reynolds stress tensor) and its dimensionality, which has to do with the morphology of the turbulence eddies, and is described by the structure dimensionality tensor $D_{ij}$. For example, if $D_{11}=0$, then the turbulence is independent of the $x_1$ axis; that is, it consists of very long structures aligned with the $x_1$ direction.

We solve analytically the RDT equations for three one-dimensional (1D) and three two-dimensional (2D) initializations in terms of the Reynolds stresses and the structure dimensionality tensor components. The simplified nonisotropic solutions are compared with the three-dimensional (3D) initially isotropic case [solved using the particle representation model (PRM) developed by Kassinos and Reynolds[23]], in order to assess their potential as a simplified qualitative representation. In fact, in the unstable regime we find good agreement for most quantities, when the initial turbulence is dependent at least on the axis of the rotation of the frame. In contrast, for the transitional and the stable regimes, the initial dependence of the turbulence on the axis of the mean flow is also necessary for good agreement. The findings of this work can be seen as additional information on the trends of the turbulence that is sheared in a rotating frame.

A strong motivation for this study arose from our efforts in developing an algebraic structure-based turbulence model, which has been successfully used, so far, to compute the characteristics of rotating turbulent channel and boundary layer flow (Kassinos *et al.*[24]). The model uses the RDT asymptotic limits as targets or guidelines, for determining the anisotropy of the Reynolds stress and structure dimensionality tensors, under strong deformations, aiming to improve the dependability and reliability. In addition, as mentioned above, in the viscous near-wall region, the turbulence structure does look much more like the asymptotic limits than like the structure in the log-layer, or in equilibrium homogeneous shear flow.

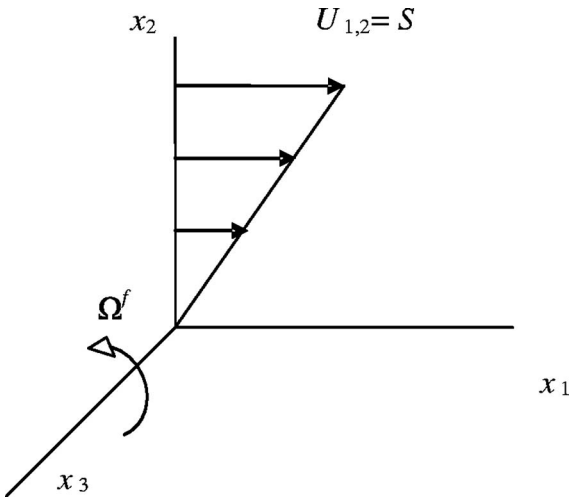


FIG. 1. Illustration of the general case for nonstratified homogeneous turbulence that is sheared in a rotating frame which is examined here.

In Sec. II of this study we present the basic linearized RDT equations for the general 3D case. In Sec. III we explain the structure dimensionality tensor and illustrate the information it carries about the morphology of the turbulence. In Sec. IV we develop the analytical solutions for the 1D and 2D alternative initializations of the original 3D problem, and in Sec. V we present the comparisons between the 3D initially isotropic solution and the alternative initializations examined here.

## II. LINEARIZED EQUATIONS

The inviscid RDT transport equations for the fluctuating velocity components $u_i$, in the case of a constant shear in a rotating frame, become (Akylas *et al.*,[21] Kassinos and Reynolds,[23] Brethouwer[4])

$$\frac{\partial u_i}{\partial t} + Sx_2\frac{\partial u_i}{\partial x_1} = -\delta_{i1}Su_2 - \frac{1}{\rho}\frac{\partial p}{\partial x_i} + \varepsilon_{ij3}2\Omega^f u_j, \tag{2.1}$$

where $S=\mathrm{d}U_1/\mathrm{d}x_2$ is the constant mean velocity gradient and $\Omega^f$ is the frame rotation rate (Fig. 1). Using the Rogallo[25] transformation, we set

$$\xi_1 = x_1 - x_2 St, \quad \xi_2 = x_2, \quad \xi_3 = x_3, \quad \tau = t, \tag{2.2}$$

and (2.1) transforms to

$$\frac{\partial u_i}{\partial \tau} = -\delta_{i1} S u_2 - \frac{1}{\rho}\frac{\partial p}{\partial \xi_i} + \delta_{i2} S\tau \frac{1}{\rho}\frac{\partial p}{\partial \xi_1} + \varepsilon_{ij3} 2\Omega^f u_j. \tag{2.3}$$

Through (2.3), the Fourier transformed variables (denoted with "∧") evolve according to

$$\frac{d\hat{u}_i}{d\tau} = -\delta_{i1} S \hat{u}_2 + \frac{i}{\rho}\hat{p}(k_i - \delta_{i2} S\tau k_1) + \varepsilon_{ij3} 2\Omega^f \hat{u}_j. \tag{2.4}$$

Applying the Fourier transformed continuity equation, i.e., $k_i \hat{u}_i = 0$, in (2.4), we can solve for the pressure

$$\frac{i}{\rho}\hat{p} = \frac{-k_1 2\Omega^f \hat{u}_2 + (k_2 - S\tau k_1) 2\Omega^f \hat{u}_1 + 2k_1 S \hat{u}_2}{k_1^2 + k_3^2 + (k_2 - S\tau k_1)^2}, \tag{2.5}$$

and by substituting into the system (2.4), this simplifies to

$$\begin{aligned}
\frac{d\hat{u}_1}{d\beta} &= \frac{-k_1 \eta \hat{u}_2 + (k_2 - k_1\beta)\eta \hat{u}_1 + 2k_1 \hat{u}_2}{k_0^2 - 2k_1 k_2 \beta + k_1^2 \beta^2} k_1 + (\eta - 1)\hat{u}_2, \\
\frac{d\hat{u}_2}{d\beta} &= \frac{-k_1 \eta \hat{u}_2 + (k_2 - k_1\beta)\eta \hat{u}_1 + 2k_1 \hat{u}_2}{k_0^2 - 2k_1 k_2 \beta + k_1^2 \beta^2} (k_2 - k_1\beta) - \eta \hat{u}_1, \\
\frac{d\hat{u}_3}{d\beta} &= \frac{-k_1 \eta \hat{u}_2 + (k_2 - k_1\beta)\eta \hat{u}_1 + 2k_1 \hat{u}_2}{k_0^2 - 2k_1 k_2 \beta + k_1^2 \beta^2} k_3,
\end{aligned} \tag{2.6}$$

where $k_0^2 = k_1^2 + k_2^2 + k_3^2$, $\beta = St$ (total shear), and $\eta = 2\Omega^f / S$. The 3D system (2.6) can be simplified for certain 1D or 2D initializations by setting specific components of the wave number vector equal to 0. In such cases, it is possible to derive analytical solutions for the evolution of the spectra of the turbulence $E_{ij} \sim \overline{\hat{u}_i \hat{u}_j^*}$, as shown in Sec. IV. By integrating the spectra over all the wave numbers, we obtain analytical expressions in physical space for the development of the stress components $R_{ij} = \overline{u_i u_j} = \int\int\int_{\mathbf{k}} E_{ij} d^3\mathbf{k}$, and the structure dimensionality tensor $D_{ij}$ (3.1), which is described in detail in the next section.

## III. THE STRUCTURE DIMENSIONALITY TENSOR

A convenient method to describe the morphology of turbulent fields is by using the one-point turbulence structure tensors, introduced by Reynolds[26] and Kassinos *et al.*[22] These tensors help to distinguish between the componentality of the turbulence (described by the Reynolds stress tensor) and its dimensionality, which has to do with the spatial structure of the turbulence eddies, and is described by the structure dimensionality tensor.

For homogeneous turbulence, the structure dimensionality tensor takes the form

$$D_{ij} = \int\int\int_{\mathbf{k}} E_{nn}(\mathbf{k}) \frac{k_i k_j}{k^2} d^3\mathbf{k}, \tag{3.1}$$

where $\mathbf{k}$ is the wave number vector, $\hat{u}_i$ are the Fourier velocity components, and $E_{ij}(\mathbf{k}) \sim \overline{\hat{u}_i \hat{u}_j^*}$ is the velocity spectrum tensor. From (3.1) it can be shown that for homogeneous turbulence,

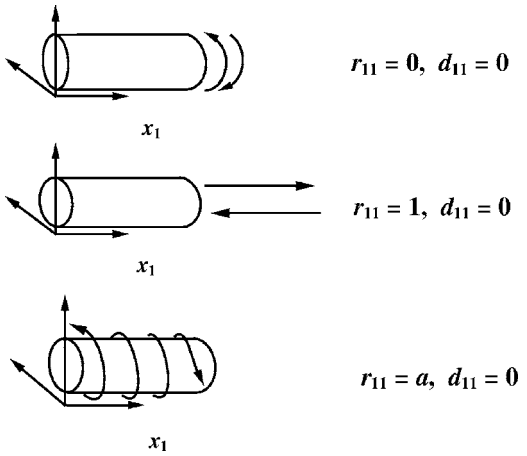


FIG. 2. Schematic diagram showing idealized 2D structures (eddies) in homogeneous turbulence and the associated componentality and dimensionality for (a) vortical eddy, (b) jetal eddy, and (c) helical eddy.

$$R_{kk} = D_{kk} = q^2, \tag{3.2}$$

where $q^2$ is twice the turbulent kinetic energy. One can define the normalized tensors

$$r_{ij} = R_{ij}/R_{kk}, \quad d_{ij} = D_{ij}/D_{kk}, \tag{3.3}$$

and it follows that their traces are

$$r_{kk} = d_{kk} = 1. \tag{3.4}$$

For isotropic turbulence, $r_{ij} = d_{ij} = \delta_{ij}/3$. In anisotropic turbulence, the combination of $r_{ij}$ and $d_{ij}$ gives a fairly detailed description of the turbulence structure. For example, $d_{11} \approx 0$ and $r_{11} \approx 0$ means that the dominant large-scale structures are very nearly 2D eddies aligned with the $x_1$ axis, with motion confined in the plane normal to the eddy axis. We call structures of this type *vortical* eddies [Fig. 2(a)]. On the other hand, $d_{11} \approx 0$ and $r_{11} \approx 1$ correspond to 2D structures (eddies) aligned with the $x_1$ axis. The motion is then confined along the eddy axis in the form of jets and wakes. We call turbulence structures of this second type *jetal* eddies [Fig. 2(b)]. A third type of turbulence structure is obtained when we have correlated jetal and vortical motion which corresponds to 2D-3C *helical* eddies [Fig. 2(c)]. In general, a turbulence field is formed by a combination of correlated vortical, jetal, and helical eddies.

Turbulence eddies can also become *flattened*; that is, their cross section can be nonaxisymmetric. The flattening of the eddies is detected by the structure dimensionality tensor, as depicted in idealized form in Fig. 3, where the eddies are assumed long in the $x_3$ direction ($d_{33} \to 0$). From the same figure it can be noticed that at the 1D limit with $d_{11} = 1$ or $d_{22} = 1$, the turbulence tends to form *sheets*, which extend perpendicularly to the $x_1$ or $x_2$ axis, respectively. Kassinos *et al.*[22,27] explored in detail the properties of the structure dimensionality tensor, using DNS data from a wide range of homogeneous and inhomogeneous flows.

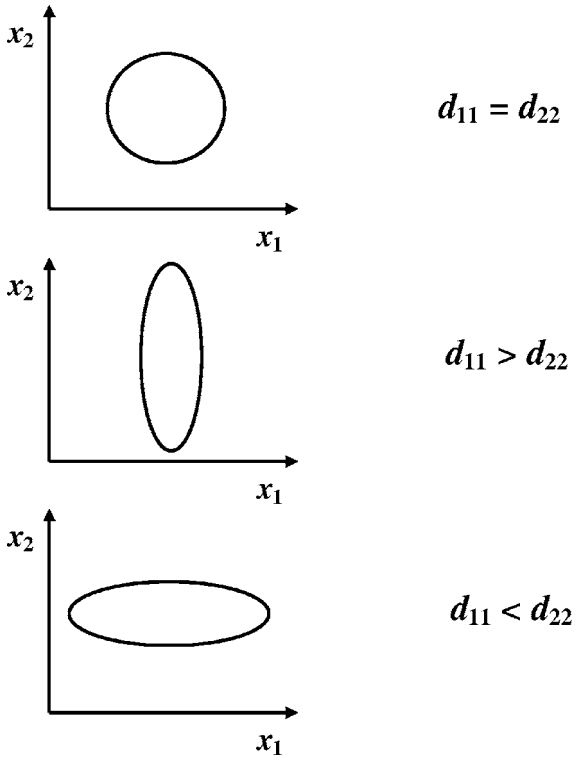


FIG. 3. Schematic diagram showing the flattening of turbulent eddies that are assumed to be elongated in the $x_3$ direction ($d_{33}\rightarrow 0$). (a) axisymmetric eddy, (b) horizontally flattened eddy, and (c) vertically flattened eddy.

## IV. ANALYTICAL SOLUTIONS FOR THE EVOLUTION OF TURBULENCE FOR VARIOUS NONISOTROPIC INITIAL CONDITIONS

As mentioned, the 3D system (2.6) can be simplified for certain 1D or 2D initializations, which implies setting specific wave numbers equal to 0, making it amenable to analytical solutions. For instance, setting $k_1=0$ means that the turbulence is initially composed of eddies that are elongated in the direction of the mean flow ($x_1$ axis). Instead of a 3D initialization, where the initial turbulence depends on all directions, we may alternatively use three different 1D (for example, corresponding to $k_2=k_3=0$) or three different 2D initializations (either $k_1$, $k_2$, or $k_3$ equals 0). In this section, we present analytical solutions of (2.6) for all these possible initial states and we discuss their characteristics in terms of the evolution of the stresses and the structure dimensionality tensor components. From the analytical solutions we calculate the RDT asymptotic states for large values of total shear $\beta$, which in fact are approached relatively fast (i.e., $\beta\sim 10$), especially for the cases in which the energy grows. As mentioned before, RDT is a meaningful approximation, when $S\tau\gg 1$ ($\tau$ is the representative eddy turn-over time scale), irrespective of the value of the total shear $\beta$. Furthermore, a comparison (Kassinos and Reynolds[7]) of the initially isotropic RDT results and LES of Bardina *et al.*[1] showed clear agreement. The RDT results are presented here in terms of the normalized stresses $r_{ij}=R_{ij}/R_{kk}$, which give information on the evolution of the componentality of the problem. The analysis extends also to the normalized structure dimensionality tensor components $d_{ij}=D_{ij}/D_{kk}$, which give information on the morphology of the turbulent field and help to describe the level of the anisotropy of the dimensionality of the turbulence.

### A. 1D-2C initializations

In the case of 1D initializations, there are three possibilities to investigate, corresponding to either $k_1$, $k_2$, or $k_3$ different than 0, which means that the turbulence depends initially on $x_1$, $x_2$, or $x_3$ axis, respectively.

#### 1. $k_1=k_2=0$, $k_3\neq 0$

This initialization corresponds to vortex sheets that are normal to the spanwise direction $x_3$. In this case, the general solution of the system (2.6) yields

$$\hat{u}_1=\frac{1}{2}\hat{u}_1^0\left(e^{\sqrt{\eta(1-\eta)}\beta}+e^{-\sqrt{\eta(1-\eta)}\beta}\right)-\frac{1}{2}\sqrt{\frac{(1-\eta)}{\eta}}\hat{u}_2^0\left(e^{\sqrt{\eta(1-\eta)}\beta}-e^{-\sqrt{\eta(1-\eta)}\beta}\right),$$

$$\hat{u}_2=\frac{1}{2}\hat{u}_2^0\left(e^{\sqrt{\eta(1-\eta)}\beta}+e^{-\sqrt{\eta(1-\eta)}\beta}\right)-\frac{1}{2}\sqrt{\frac{\eta}{(1-\eta)}}\hat{u}_1^0\left(e^{\sqrt{\eta(1-\eta)}\beta}-e^{-\sqrt{\eta(1-\eta)}\beta}\right), \tag{4.1}$$

$$\hat{u}_3=0.$$

Thus, the stresses develop as

$$R_{11}=\frac{1}{4}R_{11}^0\left(e^{\sqrt{\eta(1-\eta)}\beta}+e^{-\sqrt{\eta(1-\eta)}\beta}\right)^2+\frac{1}{4}\frac{(1-\eta)}{\eta}R_{22}^0\left(e^{\sqrt{\eta(1-\eta)}\beta}-e^{-\sqrt{\eta(1-\eta)}\beta}\right)^2,$$

$$R_{22}=\frac{1}{4}R_{22}^0\left(e^{\sqrt{\eta(1-\eta)}\beta}+e^{-\sqrt{\eta(1-\eta)}\beta}\right)^2+\frac{1}{4}\frac{\eta}{(1-\eta)}R_{11}^0\left(e^{\sqrt{\eta(1-\eta)}\beta}-e^{-\sqrt{\eta(1-\eta)}\beta}\right)^2, \tag{4.2}$$

$$R_{33}=0,$$

$$R_{12}=-\frac{1}{4}\left(\sqrt{\frac{\eta}{(1-\eta)}}R_{11}^0+\sqrt{\frac{(1-\eta)}{\eta}}R_{22}^0\right)\left(e^{\sqrt{\eta(1-\eta)}\beta}-e^{-\sqrt{\eta(1-\eta)}\beta}\right).$$

In the above, the growth of the stresses changes according to the value of $\eta$. Four cases of $\eta$ can be categorized, as described below. For all these cases, the components of the structure dimensionality tensor are zero apart from $D_{33}=R_{kk}$, which means that these solutions remain strongly 1D at all times, with all the dependence being on the axis of the frame rotation ($d_{33}=1$). Thus, the initial vortex sheets are preserved and there is a redistribution of the energy.

*a. No frame rotation,* $\eta=0$. For this case, when there is only shear and no rotation of the frame, the exponents in (4.2) are zero. By taking the appropriate limits of (4.2) at $\eta=0$, the solution for the stresses becomes

$$R_{11}=R_{11}^0+\beta^2R_{22}^0,\quad R_{22}=R_{22}^0,\quad R_{33}=0,\quad R_{12}=-\beta R_{22}^0. \tag{4.3}$$

From (4.3) it follows that the evolution of the turbulent kinetic energy is of the form $q^2\sim\beta^2$, and the initially vortical 1D-2C turbulence is driven fast to an 1D-1C state with $r_{11}\rightarrow 1$, $d_{33}=1$, resulting in the appearance of sheets extending perpendicular to the axis of the frame rotation, while the turbulent velocity aligns with the axis of the mean flow.

*b. Counter-rotating frame,* $\eta=1$. For positive values of $\eta$, the frame vorticity has the sign opposite that of the mean vorticity associated with the shear. When $\eta=1$, the frame counter-rotates at a rotation rate that matches in magnitude that of the mean shear. For this choice, through (4.2) the stresses evolve as

$$R_{11}=R_{11}^0,\quad R_{22}=R_{22}^0+\beta^2R_{11}^0,\quad R_{33}=0,\quad R_{12}=-\beta R_{11}^0. \tag{4.4}$$

Like the previous case (for $\eta=0$), the evolution of the turbulent kinetic energy when $\eta=1$, is of the form $q^2\sim\beta^2$ and the asymptotic state for the turbulence is 1D-1C with $r_{22}\rightarrow 1$, $d_{33}=1$. Thus, the resulting structure corresponds to sheets normal to the rotation axis but with the velocity components aligned with the direction $x_2$.

*c. Counter-rotating frame,* $0<\eta<1$. When $\eta$ lies between 0 and 1, the frame is counter-rotating at a rate that is smaller than the rotation rate associated with the mean shear itself. This is the unstable regime where the turbulent kinetic energy grows exponentially with time, since the exponents in (4.2) are nonzero real numbers. From (4.2) it follows that for large $\beta$, the turbulent kinetic energy grows as $q^2\sim\exp 2\sqrt{\eta(1-\eta)}\beta$ and, for a vortical initialization with $R_{11}^0=R_{22}^0=q_0^2/2$, the turbulence reaches asymptotically a 2C-1D state with $r_{11}\rightarrow(1-\eta)$, $r_{22}\rightarrow\eta$, $d_{33}=1$. This state corresponds to sheets perpendicular to the axis of the frame rotation with the fluctuating velocities being inclined to the other two axes at an angle that depends on $\eta$.

*d. Co-rotating, and counter-rotating at high rates:* $\eta<0$, *and* $\eta>1$. We consider now the case when the frame is rotating with the same direction as the mean rotation associated with the mean shear or counter-rotating at a rate that exceeds the one associated with the mean shear. For these cases, the exponents in (4.2) become imaginary numbers and thus, the solution characterizes a stable energy regime where the stresses show an oscillating behavior. From (4.2) we may conclude that when starting with the vortical 1D-2C state, i.e., $R_{11}^0=R_{22}^0=q_0^2/2$, the turbulent kinetic energy evolves as $R_{ii}/q_0^2=\{4\eta(\eta-1)+1-\cos[2\sqrt{\eta(\eta-1)}\beta]\}/4\eta(\eta-1)$. The turbulence has a 2C-1D character, since $d_{33}=1$ and the normalized stresses oscillate around the values $r_{11}\rightarrow(\eta-1)/(2\eta-1)$, $r_{22}\rightarrow\eta/(2\eta-1)$, $r_{33}=0$. This state corresponds to sheets perpendicular to the axis of the frame rotation and turbulent velocities that oscillate about a mean angle of inclination, relative to the other two axes, which depends on $\eta$.

#### 2. $k_2=k_3=0$, $k_1\neq 0$

For this initialization, the transformed components are independent of $\eta$, in agreement with the principle of *material indifference* (Speziale[28]) for turbulent motion independent of the direction of the frame rotation ($k_3=0$). The stresses (except $R_{33}$, which remains constant) show a diminishing behavior of the following form:

$$R_{11}=\frac{\beta^2}{(1+\beta^2)^2}R_{22}^0,\quad R_{22}=\frac{1}{(1+\beta^2)^2}R_{22}^0,$$
$$R_{33}=R_{33}^0,\quad R_{12}=\frac{\beta}{(1+\beta^2)^2}R_{22}^0, \tag{4.5}$$

where the superscript "0" is used to denote an initial value. The development of the structure dimensionality tensor components

$$D_{11}=\frac{R_{22}^0}{(1+\beta^2)^2}+\frac{R_{33}^0}{1+\beta^2},\quad D_{22}=D_{11}\beta^2,\quad D_{33}=0, \tag{4.6}$$

imply that, although this initialization starts as 1D depending only on the $x_1$ direction $[d_{11}(0)=1]$, it evolves as 2D, forming helical eddies that are gradually flattened along the $x_2$ axis and approaches finally an 1D state, resulting in sheets that develop perpendicular to the axis of the gradient of the mean velocity ($d_{22}\rightarrow 1$). The velocity fluctuations are aligned with the axis of the frame rotation ($r_{33}\rightarrow 1$).

#### 3. $k_1=k_3=0$, $k_2\neq 0$

In this case, unlike the previous ones, the stresses and the structure dimensionality tensor components are constant, and thus the turbulence remains fixed in its initial state, independent of $\eta$ and $\beta$. Again, this is consistent with the expected material indifference of 2D turbulence, which is independent of the direction of the frame rotation.

### B. 2D-3C initializations

We now turn to the 2D initializations for which there are three options, with either $k_1$, $k_2$, or $k_3$ equal to zero. When the componentality of the initially 2D turbulence is isotropic in planes perpendicular to the axis of independence $x_\ell$ ($\ell=1$, 2, or 3), the initial turbulence is vortical and its spectrum is given by (no summation implied by repeated indices)

$$E_{ij}^0(k_0)=\frac{E(k_0)}{2\pi k}\left(\delta_{ij}-\frac{k_ik_j}{k_0^2}\right)(1-\delta_{i\ell})(1-\delta_{j\ell}), \tag{4.7}$$

for $i=1,2,3$, $j=1,2,3$.

Another possibility is for the initial turbulence to be completely jetal, with all the velocity fluctuations being in the direction of the axis of independence $x_\ell$. The initial jetal spectrum corresponding to this condition is (no summation implied by repeated indices)

$$E_{ij}^0(k_0) = \frac{E(k_0)}{2\pi k_0}\delta_{i\ell}\delta_{j\ell}, \quad \text{for} \quad i=1,2,3, \quad j=1,2,3. \tag{4.8}$$

In the relations (4.7) and (4.8) the initial turbulent kinetic energy spectrum $E(k_0)$ satisfies

$$\int_{k_0=0}^{\infty} E(k_0)dk_0 = \frac{q_0^2}{2} = \frac{R_{ii}^0}{2}. \tag{4.9}$$

Because of the linearity of the governing equations, the solutions for the initially jetal 2D-1C and the vortical 2D-2C cases can be superimposed to produce $R_{ij}$ and $D_{ij}$ for various 2D-3C initial fields consisting of uncorrelated jets and vortices.

### 1. $k_3=0$

In this case, where the turbulence is independent of the axis of the frame rotation, the system (2.6) becomes independent of $\eta$, consistent with the principle of material indifference of 2D turbulence,[28] and the spectral solution yields

$$E_{11} = \frac{k_0^4[E_{11}^0 + \beta^2 E_{22}^0 + \beta(E_{12}^0 + E_{21}^0)]}{[k_1^2 + (k_2 - k_1\beta)^2]^2},$$

$$E_{22} = \frac{k_0^4 E_{22}^0}{[k_1^2 + (k_2 - k_1\beta)^2]^2}, \tag{4.10}$$

$$E_{33} = E_{33}^0, \quad E_{12} = \frac{k_0^4\beta E_{22}^0 + k_0^4 E_{12}^0}{[k_1^2 + (k_2 - k_1\beta)^2]^2}.$$

From the above, it is apparent that the jetal initialization results in a constant turbulent kinetic energy state, with all the stresses zero apart from $R_{33}$:

$$R_{11}^{\text{jet}}/q_0^2 = 0, \quad R_{22}^{\text{jet}}/q_0^2 = 0, \quad R_{33}^{\text{jet}}/q_0^2 = 1, \quad R_{12}^{\text{jet}}/q_0^2 = 0. \tag{4.11}$$

However, by integrating (3.1) we find that the dimensionality structure tensor components evolve as

$$D_{11}^{\text{jet}} = \frac{2}{4+\beta^2}q_0^2, \quad D_{22}^{\text{jet}} = \frac{2+\beta^2}{4+\beta^2}q_0^2,$$

$$D_{33}^{\text{jet}} = 0, \quad D_{12}^{\text{jet}} = -\frac{2+\beta^2}{4\beta+\beta^3}q_0^2, \tag{4.12}$$

and as a result, the jetal initialization approaches a 1D-1C state with $r_{33}^{\text{jet}}=1$, $d_{22}^{\text{jet}}\to 1$, forming sheets that develop perpendicular to the $x_2$ axis (axis of the gradient of the mean velocity).

On the other hand, when the initially vortical velocity spectrum tensor (4.7) is used, the integrations produce a constant state:

$$R_{11}^{\text{vor}} = D_{11}^{\text{vor}} = q_0^2/2, \quad R_{22}^{\text{vor}} = D_{22}^{\text{vor}} = q_0^2/2,$$

$$R_{33}^{\text{vor}} = D_{33}^{\text{vor}} = 0, \quad R_{12}^{\text{vor}} = D_{12}^{\text{vor}} = 0. \tag{4.13}$$

As a result, initially vortical 2D-2C turbulence which is initially independent on the axis of the rotation of the frame remains unaffected by mean shear and rotation.

### 2. $k_1=0$

When the turbulence is initially independent of the direction of the mean flow, thus consisting of elongated eddies aligned with the streamwise direction, the general solution of (2.6) reads

$$\hat{u}_1 = \hat{u}_1^0 \cosh\left(\frac{k_3}{k}\sqrt{\eta(1-\eta)}\beta\right) - \hat{u}_2^0\sqrt{\frac{1-\eta}{\eta}}\frac{k}{k_3}\sinh\left(\frac{k_3}{k}\sqrt{\eta(1-\eta)}\beta\right),$$

$$\hat{u}_2 = \hat{u}_2^0 \cosh\left(\frac{k_3}{k}\sqrt{\eta(1-\eta)}\beta\right) - \hat{u}_1^0\sqrt{\frac{\eta}{1-\eta}}\frac{k_3}{k}\sinh\left(\frac{k_3}{k}\sqrt{\eta(1-\eta)}\beta\right), \tag{4.14}$$

$$\hat{u}_3 = \hat{u}_1^0\sqrt{\frac{\eta}{1-\eta}}\frac{k_2}{k}\sinh\left(\frac{k_3}{k}\sqrt{\eta(1-\eta)}\beta\right) - \frac{k_2}{k_3}\hat{u}_2^0\cosh\left(\frac{k_3}{k}\sqrt{\eta(1-\eta)}\beta\right),$$

and, in the case of the initially vortical velocity spectrum, the integration of (4.7) results in the following evolution of the stress components:

$$\frac{R_{11}^{\text{vor}}}{q_0^2} = \frac{1}{2}\frac{1-\eta}{\eta}\{-1 + I_0[2\sqrt{\eta(1-\eta)}\beta]\},$$

$$\frac{R_{22}^{\text{vor}}}{q_0^2} = \frac{1}{4} + \frac{I_0[2\sqrt{\eta(1-\eta)}\beta]}{2} - \frac{I_1[2\sqrt{\eta(1-\eta)}\beta]}{4\sqrt{\eta(1-\eta)}\beta},$$

$$\frac{R_{33}^{\text{vor}}}{q_0^2} = \frac{1}{4} + \frac{I_1[2\sqrt{\eta(1-\eta)}\beta]}{4\sqrt{\eta(1-\eta)}\beta}, \tag{4.15}$$

$$\frac{R_{12}^{\text{vor}}}{q_0^2} = -\frac{1}{2}\sqrt{\frac{1-\eta}{\eta}}I_1[2\sqrt{\eta(1-\eta)}\beta],$$

where $I_n$ are Bessel functions of the first kind. From (4.15), the turbulent kinetic energy evolves as

$$\frac{R_{ii}^{\text{vor}}}{q_0^2} = \left[-\frac{1-2\eta}{2\eta} + \frac{1}{2\eta}I_0[2\sqrt{\eta(1-\eta)}\beta]\right]. \tag{4.16}$$

Similarly, the components of the structure dimensionality tensor are

$$D_{11}^{\mathrm{vor}}=0,\quad \frac{D_{22}^{\mathrm{vor}}}{q_0^2}=\frac{2\eta-1}{4\eta}+\frac{I_1[2\sqrt{\eta(1-\eta)}\beta]}{4\eta\sqrt{\eta(1-\eta)}\beta},\quad D_{12}^{\mathrm{vor}}=0,$$
$$\frac{D_{33}^{\mathrm{vor}}}{q_0^2}=\frac{2\eta-1}{4\eta}+\frac{1}{2\eta}I_0[2\sqrt{\eta(1-\eta)}\beta]-\frac{I_1[2\sqrt{\eta(1-\eta)}\beta]}{4\eta\sqrt{\eta(1-\eta)}\beta}. \tag{4.17}$$

When a jetal initialization is used, the solutions for the stresses [through (4.8)] become

$$\frac{R_{11}^{\mathrm{jet}}}{q_0^2}=\frac{1}{2}+\frac{I_0[2\sqrt{\eta(1-\eta)}\beta]}{2},$$
$$\frac{R_{22}^{\mathrm{jet}}}{q_0^2}=\frac{\eta}{1-\eta}\left[-\frac{1}{4}+\frac{I_0[2\sqrt{\eta(1-\eta)}\beta]}{2}-\frac{I_1[2\sqrt{\eta(1-\eta)}\beta]}{4\sqrt{\eta(1-\eta)}\beta}\right],$$
$$\frac{R_{33}^{\mathrm{jet}}}{q_0^2}=\frac{\eta}{1-\eta}\left[-\frac{1}{4}+\frac{I_1[2\sqrt{\eta(1-\eta)}\beta]}{4\sqrt{\eta(1-\eta)}\beta}\right], \tag{4.18}$$
$$\frac{R_{12}^{\mathrm{jet}}}{q_0^2}=-\frac{1}{2}\sqrt{\frac{\eta}{1-\eta}}I_1[2\sqrt{\eta(1-\eta)}\beta],$$

and the trace evolves as

$$\frac{R_{ii}^{\mathrm{jet}}}{q_0^2}=\frac{1-2\eta}{2(1-\eta)}+\frac{1}{2(1-\eta)}I_0[2\sqrt{\eta(1-\eta)}\beta]. \tag{4.19}$$

In addition, the dimensionality structure tensor is calculated as

$$D_{11}^{\mathrm{jet}}=0,\quad \frac{D_{22}^{\mathrm{jet}}}{q_0^2}=\frac{1-2\eta}{4(1-\eta)}+\frac{I_1[2\sqrt{\eta(1-\eta)}\beta]}{4(1-\eta)\sqrt{\eta(1-\eta)}\beta},\quad D_{12}^{\mathrm{jet}}=0,$$
$$\frac{D_{33}^{\mathrm{jet}}}{q_0^2}=\frac{1-2\eta}{4(1-\eta)}+\frac{1}{2(1-\eta)}I_0[2\sqrt{\eta(1-\eta)}\beta]-\frac{I_1[2\sqrt{\eta(1-\eta)}\beta]}{4(1-\eta)\sqrt{\eta(1-\eta)}\beta}. \tag{4.20}$$

As in the 1D initialization with $k_1=k_2=0$, we may categorize the dependence of the solution of $\eta$ in the same four categories.

*a. No frame rotation,* $\eta=0$. For this case, when there is only shear and no rotation, the arguments in the Bessel functions in equations (4.15)–(4.20) are zero. In the vortical case, from (4.15) and (4.17) we calculate

$$R_{11}^{\mathrm{vor}}=q_0^2\beta^2/2,\quad R_{22}^{\mathrm{vor}}=q_0^2/2,$$
$$R_{33}^{\mathrm{vor}}=q_0^2/2,\quad R_{12}^{\mathrm{vor}}=-q_0^2\beta/2,$$
$$D_{11}^{\mathrm{vor}}=0,\quad D_{22}^{\mathrm{vor}}=q_0^2(1+\beta^2/4), \tag{4.21}$$
$$D_{33}^{\mathrm{vor}}=q_0^2(1+3\beta^2/4),\quad D_{12}^{\mathrm{vor}}=0.$$

From Eqs. (4.21) we may note that at large total shear $\beta$, the normalized stresses $r_{ij}=R_{ij}/R_{kk}$ and structure dimensionality tensor components $d_{ij}=D_{ij}/R_{kk}$, become

$$r_{11}^{\mathrm{vor}}\to 1,\quad d_{22}^{\mathrm{vor}}\to 1/4,\quad d_{33}^{\mathrm{vor}}\to 3/4. \tag{4.22}$$

This means that the initially 2D vortical turbulence is driven to jetal turbulence, with eddies flattened along the $x_3$ axis.

In the case of initially jetal turbulence, the limits of (4.18) and (4.20) result in a constant state equal to the initial one, and as a result, the 3C solution obtained through the superposition of the vortical and the jetal parts is dominated by the vortical part.

*b. Counter-rotating frame,* $\eta=1$. When $\eta=1$, the frame counter rotates at a rate that is equal in magnitude to the intrinsic rotation of the mean shear. As in the previous case, the arguments in the Bessel functions in Eqs. (4.15)–(4.20) vanish. Using a vortical initial spectrum, we find that the one-point statistics of the initially vortical turbulence [Eqs. (4.15) and (4.17)] remain completely unaffected by the combined action of the mean shear and the frame rotation. However, when the initial jetal spectrum is used, the turbulent stresses (4.18) and the structure dimensionality tensor components (4.20) evolve according to

$$R_{11}^{\mathrm{jet}}=q_0^2,\quad R_{22}^{\mathrm{jet}}=3q_0^2\beta^2/8,$$
$$R_{33}^{\mathrm{jet}}=q_0^2\beta^2/8,\quad R_{12}^{\mathrm{jet}}=-q_0^2\beta/2,$$
$$D_{11}^{\mathrm{jet}}=0,\quad D_{22}^{\mathrm{jet}}=q_0^2(1/2+\beta^2/8), \tag{4.23}$$
$$D_{33}^{\mathrm{jet}}=q_0^2(1/2+3\beta^2/8),\quad D_{12}^{\mathrm{jet}}=0.$$

From Eqs. (4.23), it follows that as the total shear $\beta$ increases, the normalized stresses $r_{ij}=R_{ij}/R_{kk}$ and the normalized structure dimensionality tensor components $d_{ij}=D_{ij}/R_{kk}$ tend to the following 2D-2C state:

$$r_{22}^{\mathrm{jet}}\to 3/4,\quad r_{33}^{\mathrm{jet}}\to 1/4,\quad d_{22}^{\mathrm{jet}}\to 1/4,\quad d_{33}^{\mathrm{jet}}\to 3/4, \tag{4.24}$$

which means that when $\eta=1$ the mean shear drives 2D initially jetal turbulence to a vortical state with flattened structures and unequal distribution of the energy between the directions normal to the axis of the mean flow.

*c. Counter-rotating frame,* $0<\eta<1$. This case is when the frame is counter-rotating at a rate that is smaller than the rotation rate associated with the mean shear itself. For these cases the arguments in the Bessel functions in (4.15)–(4.20) are nonzero positive real numbers. In the limit of infinite total shear, for a vortical initialization, the normalized stresses and the structure dimensionality tensor components tend to a 1D-2C state with

$$r_{11}^{\mathrm{vor}} \to 1-\eta, \quad r_{22}^{\mathrm{vor}} \to \eta, \quad r_{33}^{\mathrm{vor}} \to 0, \quad r_{12}^{\mathrm{vor}} \to -\sqrt{\eta(1-\eta)},$$
$$d_{11}^{\mathrm{vor}} \to 0, \quad d_{22}^{\mathrm{vor}} \to 0, \quad d_{33}^{\mathrm{vor}} \to 1, \quad d_{12}^{\mathrm{vor}} \to 0. \tag{4.25}$$

All the dependence is confined along the axis of the frame rotation, while the distribution of the energy in the plane normal to the axis depends on the actual value of $\eta$. Such a state corresponds to sheets extending perpendicular to the axis of the frame rotation and turbulent motion aligning with the other two directions.

For a jetal initialization, from the equations (4.18)–(4.20) it follows that the asymptotic behavior of the normalized stress and the structure dimensionality tensor components are

$$r_{11}^{\mathrm{jet}} \to 1-\eta, \quad r_{22}^{\mathrm{jet}} \to \eta, \quad r_{33}^{\mathrm{jet}} \to 0, \quad r_{12}^{\mathrm{jet}} \to -\sqrt{\eta(1-\eta)},$$
$$d_{11}^{\mathrm{jet}} \to 0, \quad d_{22}^{\mathrm{jet}} \to 0, \quad d_{33}^{\mathrm{jet}} \to 1, \quad d_{12}^{\mathrm{jet}} \to 0. \tag{4.26}$$

As a result, shear in a frame counter-rotating at a rate that is smaller than the mean rotation due to the shear, drives 2D-1C initially jetal turbulence to the same 1D-2C state of sheets that was found to be the fixed state for initially vortical turbulence [Eq. (4.25)]. The same asymptotic states for the normalized stresses and the structure dimensionality tensor components have also been calculated by the 1D analysis with all the dependence on the axis of the frame rotation ($k_3 \neq 0$).

*d. Co-rotating, and counter-rotating at high rates:* $\eta < 0$, *and* $\eta > 1$. This case is when the frame is counter-rotating at a rate that is smaller than the rotation rate associated with the mean shear itself. For these cases the argument $\sqrt{\eta(1-\eta)}$ in the Bessel functions in (4.15)–(4.20) is an imaginary number. In that case, we can change the argument to a real number, making use of the relations

$$I_0[2\sqrt{\eta(1-\eta)}\beta] = J_0[2\sqrt{\eta(\eta-1)}\beta] \tag{4.27}$$

and

$$I_1[2\sqrt{\eta(1-\eta)}\beta] = iJ_1[2\sqrt{\eta(\eta-1)}\beta], \tag{4.28}$$

where $J_n$ are Bessel functions of the second kind, and $i$ is the imaginary unit. The $J_n$ oscillate with decreasing amplitude as their argument increases:

$$J_0(z) \approx \sqrt{\frac{2\pi}{z}}[\cos(z-\pi/4)+\cdots], \quad \text{for} \quad z \to \infty,$$
$$J_1(z) \approx \sqrt{\frac{2\pi}{z}}[\cos(z-3\pi/4)+\cdots], \tag{4.29}$$

and therefore at large total shear the normalized stresses and the normalized structure dimensionality tensor components attain the asymptotic values

$$r_{11}^{\mathrm{vor}} \to \frac{\eta-1}{2\eta-1}, \quad r_{22}^{\mathrm{vor}} \to \frac{\eta}{2(2\eta-1)},$$
$$r_{33}^{\mathrm{vor}} \to \frac{\eta}{2(2\eta-1)}, \quad r_{12}^{\mathrm{vor}} \to 0, \tag{4.30}$$
$$d_{11}^{\mathrm{vor}} \to 0, \quad d_{22}^{\mathrm{vor}} \to 1/2, \quad d_{33}^{\mathrm{vor}} \to 1/2, \quad d_{12}^{\mathrm{vor}} \to 0.$$

As a result, mean shear in a co-rotating frame ($\eta < 0$) or in a counter-rotating frame at high rotation rates ($\eta > 1$) drives 2D-2C initially vortical turbulence to a 2D-3C state with axisymmetric structures and an equipartition of energy within the plane normal to the axis of independence (axis of the mean flow). The final distribution of the energy along ($r_{11}$) and normal ($r_{22}, r_{33}$) to this axis depends on the value of $\eta$.

When the initial turbulence consists of fluctuations along the axis of independence, the initial jetal velocity spectrum tensor is given by (4.8). Using this initial spectrum, one finds that again, because of the decreasing amplitude of the Bessel functions for large arguments, for large total shear the normalized tensor components approach the following limits:

$$r_{11}^{\mathrm{jet}} \to \frac{\eta-1}{2\eta-1}, \quad r_{22}^{\mathrm{jet}} \to \frac{\eta}{2(2\eta-1)},$$
$$r_{33}^{\mathrm{jet}} \to \frac{\eta}{2(2\eta-1)}, \quad r_{12}^{\mathrm{jet}} \to 0, \tag{4.31}$$
$$d_{11}^{\mathrm{jet}} \to 0, \quad d_{22}^{\mathrm{jet}} \to 1/2, \quad d_{33}^{\mathrm{jet}} \to 1/2, \quad d_{12}^{\mathrm{jet}} \to 0.$$

As a result, mean shear drives 2D initially jetal turbulence to the same 2D-3C state that was observed for initially 2D-2C vortical turbulence. In terms of the morphology of the turbulence, this state differs from the respective one found from the 1D solution with $k_3 \neq 0$ described in Sec. IV A 3. However, we may note the equality between the respective asymptotic states for $r_{11}$ as well as the similarity of the resulting oscillating behavior for the turbulent kinetic energy.

### 3. $k_2 = 0$

This case starts as 2D and migrates to 3D since the shear forms (in real space) $k_2'(\beta) = -k_1\beta$; thus, it is as close as possible to the fully 3D initially isotropic case. For this choice (more complicated compared to the previous ones), the system (2.6) yields for the evolution of $\hat{u}_2$,

$$\frac{d^2\hat{u}_2}{d\beta^2}(1+\beta^2\cos^2\theta) + \frac{d\hat{u}_2}{d\beta}(4\beta\cos^2\theta) + \hat{u}_2[\eta(\eta-1)\sin^2\theta + 2\cos^2\theta] = 0, \tag{4.32}$$

where we made use of cylindrical coordinates, substituting $k_1 = k_0\cos\theta$ and $k_3 = k_0\sin\theta$. Combining Eqs. (2.6) and (4.32), we obtain the solutions for the Fourier transformed velocity components, and the corresponding velocity spectra in the case of an initially vortical turbulence become

TABLE I. Asymptotic limits for the normalized stresses $r_{ij}$ and structure dimensionality tensor components $d_{ij}$, and the turbulent kinetic energy $q^2/q_0^2$, at large total shear, for the various initializations examined in the unstable regime ($B>0$). For the 1D-2C cases a vortical initial state has been used, while for the 2D-3C, a superposition equally weighted between the vortical and the jetal part of the solution.

| Initialization | | $r_{11}$ | $r_{22}$ | $r_{33}$ | $r_{12}$ | $d_{11}$ | $d_{22}$ | $d_{33}$ | $d_{12}$ | $q^2/q_0^2$ |
|---|---|---|---|---|---|---|---|---|---|---|
| 1D-2C | $k_1\neq 0$ | 0 | 0 | 1 | 0 | 0 | 1 | 0 | 0 | 1/2 |
| | $k_2\neq 0$ | 1/2 | 0 | 1/2 | 0 | 0 | 1 | 0 | 0 | 1 |
| | $k_3\neq 0$ | $1-\eta$ | $\eta$ | 0 | $-B^{1/2}$ | 0 | 0 | 1 | 0 | $\sim\exp(2\beta B^{1/2})$ |
| 2D-3C | $k_3=0$ | 1/4 | 1/4 | 1/2 | 0 | 1/4 | 3/4 | 0 | 0 | 1 |
| | $k_1=0$ | $1-\eta$ | $\eta$ | 0 | $-B^{1/2}$ | 0 | 0 | 1 | 0 | $\sim\beta^{-1/2}\exp(2\beta B^{1/2})$ |
| | $k_2=0$ | $1-\eta$ | $\eta$ | 0 | $-B^{1/2}$ | 0 | 0 | 1 | 0 | $\sim\beta^{-3/2}\exp(2\beta B^{1/2})$ |
| 3D-3C isotropic | | $1-\eta$ | $\eta$ | 0 | $-B^{1/2}$ | 0 | 0 | 1 | 0 | $\sim\beta^{-2}\exp(2\beta B^{1/2})$ |

$$
\begin{aligned}
E_{11} &= [1-\beta^2\cos^2\theta(\eta-3)]^2 F_1^2(5/4-a;5/4+a;3/2;-\beta^2\cos^2\theta)E_{11}^0 + (25/12-4/3a^2)^2\beta^4\cos^4\theta \\
&\quad\times F_1^2(9/4-a;9/4+a;5/2;-\beta^2\cos^2\theta)E_{11}^0 - 2\beta^2\cos^2\theta[1-\beta^2\cos^2\theta(\eta-3)]F_1(9/4-a;9/4+a;5/2;-\beta^2\cos^2\theta) \\
&\quad\times(25/12-4/3a^2)F_1(5/4-a;5/4+a;3/2;-\beta^2\cos^2\theta)E_{11}^0,
\end{aligned}
$$

$$
E_{22} = \eta^2\beta^2 F_1^2(5/4-a;5/4+a;3/2;-\beta^2\cos^2\theta)E_{11}^0,
$$

$$
\begin{aligned}
E_{33} &= \beta^4\cos^4\theta\cot^2\theta(1+\beta^2\cos^2\theta)^2(25/12-4/3a^2)^2F_1^2(9/4-a;9/4+a;5/2;-\beta^2\cos^2\theta)E_{11}^0 \\
&\quad + (1+\eta\beta^2\sin^2\theta+3\beta^2\cos^2\theta)^2\cot^2\theta F_1^2(5/4-a;5/4+a;3/2;-\beta^2\cos^2\theta)E_{11}^0 \\
&\quad - 2\beta^2\cos^2\theta\cot^2\theta(1+\beta^2\cos^2\theta)(1+\eta\beta^2\sin^2\theta+3\beta^2\cos^2\theta)(25/12-4/3a^2) \\
&\quad\times F_1(9/4-a;9/4+a;5/2;-\beta^2\cos^2\theta)F_1(5/4-a;5/4+a;3/2;-\beta^2\cos^2\theta)E_{11}^0,
\end{aligned}
$$

$$
\begin{aligned}
E_{12} &= -\eta\beta[1-\beta^2\cos^2\theta(\eta-3)]F_1^2(5/4-a;5/4+a;3/2;-\beta^2\cos^2\theta)E_{11}^0 + \eta\beta^3\cos^2\theta(1+\beta^2\cos^2\theta) \\
&\quad\times F_1(9/4-a;9/4+a;5/2;-\beta^2\cos^2\theta)(25/12-4/3a^2)F_1(5/4-a;5/4+a;3/2;-\beta^2\cos^2\theta)E_{11}^0,
\end{aligned}
$$

(4.33)

where $F_1$ is the hypergeometric function, with the parameter $\alpha$ given by

$$
a = [\sqrt{1+4\eta(1-\eta)\tan^2\theta}]/4. \tag{4.34}
$$

In the case of the initially jetal velocity distribution, the spectral solution is

TABLE II. As in Table I, but at the transitional regime, for $\eta=0$.

| Initialization | | $r_{11}$ | $r_{22}$ | $r_{33}$ | $r_{12}$ | $d_{11}$ | $d_{22}$ | $d_{33}$ | $d_{12}$ | $q^2/q_0^2$ |
|---|---|---|---|---|---|---|---|---|---|---|
| 1D-2C | $k_1\neq 0$ | 0 | 0 | 1 | 0 | 0 | 1 | 0 | 0 | 1/2 |
| | $k_2\neq 0$ | 1/2 | 0 | 1/2 | 0 | 0 | 1 | 0 | 0 | 1 |
| | $k_3\neq 0$ | 1 | 0 | 0 | 0 | 0 | 0 | 1 | 0 | $\sim\beta^2$ |
| 2D-3C | $k_3=0$ | 1/4 | 1/4 | 1/2 | 0 | 1/4 | 3/4 | 0 | 0 | 1 |
| | $k_1=0$ | 1 | 0 | 0 | 0 | 0 | 1/4 | 3/4 | 0 | $\sim\beta^2$ |
| | $k_2=0$ | 1 | 0 | 0 | 0 | 0 | $\sim$0.6 | $\sim$0.4 | 0 | $\sim\beta$ |
| 3D-3C isotropic | | 1 | 0 | 0 | 0 | 0 | $\sim$0.7 | $\sim$0.3 | 0 | $\sim\beta$ |

TABLE III. As in Table I, but at the transitional regime, for $\eta=1$.

| Initialization | | $r_{11}$ | $r_{22}$ | $r_{33}$ | $r_{12}$ | $d_{11}$ | $d_{22}$ | $d_{33}$ | $d_{12}$ | $q^2/q_0^2$ |
|---|---|---|---|---|---|---|---|---|---|---|
| 1D-2C | $k_1\neq 0$ | 0 | 0 | 1 | 0 | 0 | 1 | 0 | 0 | 1/2 |
| | $k_2\neq 0$ | 1/2 | 0 | 1/2 | 0 | 0 | 1 | 0 | 0 | 1 |
| | $k_3\neq 0$ | 0 | 1 | 0 | 0 | 0 | 0 | 1 | 0 | $\sim\beta^2$ |
| 2D-3C | $k_3=0$ | 1/4 | 1/4 | 1/2 | 0 | 1/4 | 3/4 | 0 | 0 | 1 |
| | $k_1=0$ | 0 | 1/4 | 3/4 | 0 | 0 | 3/4 | 1/4 | 0 | $\sim\beta^2$ |
| | $k_2=0$ | 0 | 1/2 | 1/2 | 0 | 0 | 1/2 | 1/2 | 0 | $\sim\beta$ |
| 3D-3C isotropic | | 0 | 1/2 | 1/2 | 0 | 0 | 1/2 | 1/2 | 0 | $\sim\beta$ |

$$
\begin{aligned}
\eta^2 E_{11} &= (\eta-2)^2\beta^2\cos^4\theta\, F_1^2(3/4-a;3/4+a;1/2;-\beta^2\cos^2\theta)E_{22}^0+\beta^2(1+\beta^2\cos^2\theta)^2\cos^4\theta(9/4-4a^2)^2\\
&\quad\times F_1^2(7/4-a;7/4+a;3/2;-\beta^2\cos^2\theta)E_{22}^0+2(\eta-2)\beta^2\cos^4\theta(1+\beta^2\cos^2\theta)F_1(7/4-a;7/4+a;1/2;-\beta^2\cos^2\theta)\\
&\quad\times(9/4-4a^2)F_1(3/4-a;3/4+a;3/2;-\beta^2\cos^2\theta)E_{22}^0,\\
\eta^2 E_{22} &= \eta^2 F_1^2(3/4-a;3/4+a;1/2;-\beta^2\cos^2\theta)E_{22}^0,\\
\eta^2 E_{33} &= \beta^2[(\eta-2)\sin^2\theta+2]^2\cot^2\theta F_1^2(3/4-a;3/4+a;1/2;-\beta^2\cos^2\theta)E_{22}^0+\beta^2(1+\beta^2\cos^2\theta)^2\cos^4\theta\\
&\quad\times\cot^2\theta(9/4-4a^2)^2F_1^2(7/4-a;7/4+a;3/2;-\beta^2\cos^2\theta)E_{22}^0-2\beta^2[(\eta-2)\sin^2\theta+2](1+\beta^2\cos^2\theta)\cos^2\theta\\
&\quad\times\cot^2\theta(9/4-4a^2)F_1(3/4-a;3/4+a;1/2;-\beta^2\cos^2\theta)F_1(7/4-a;7/4+a;3/2;-\beta^2\cos^2\theta)E_{22}^0,\\
\eta E_{12} &= (\eta-2)\beta\cos^2\theta\, F_1^2(3/4-a;3/4+a;1/2;-\beta^2\cos^2\theta)E_{22}^0+\beta(1+\beta^2\cos^2\theta)\cos^2\theta(9/4-4a^2)\\
&\quad\times F_1(7/4-a;7/4+a;3/2;-\beta^2\cos^2\theta)F_1(3/4-a;3/4+a;1/2;-\beta^2\cos^2\theta)E_{22}^0.
\end{aligned}
\tag{4.35}
$$

Due to the complexity of the above relations, we perform numerical integrations (presented in Sec. V) of the spectral solutions (from $\theta=0$ to $\pi$), for the derivation of the stresses and the structure dimensionality tensor components. However, we may recover some of the basic qualitative characteristics regarding the evolution of the turbulent kinetic energy, through a rough investigation of the above defined spectral solutions. In the unstable regime, when $0<\eta<1$, $a$ is a real function of $\theta$ and, as a result, the stresses show an exponential growth with time, which agrees with the findings from the 2D initialization with $k_1=0$ and the 1D initialization with $k_3\neq 0$. For values of $\eta$ less than 0 or bigger than 1, corresponding to the stable cases, $a$ is complex, and the stresses show a decreasing behavior with diminishing oscillations. The decrease of the energy in this regime cannot be described by the other two initializations, where only an oscillating behavior is present, as discussed.

For the cases when $\eta=0$ or 1, $a$ equals 1/4, leading into a linear growth of the kinetic energy, as it will be shown. For the specific case when the frame counter-rotates ($\eta=1$), a simple analytical solution in real space can be derived. For this specific choice of $\eta=1$, and for an initially vortical turbulence the integration of the spectral solution (4.33) is simplified, and we derive final expressions for the $R_{ij}$:

TABLE IV. As in Table I, but at the stable regime ($B<0$).

| Initialization | | $r_{11}$ | $r_{22}$ | $r_{33}$ | $r_{12}$ | $d_{11}$ | $d_{22}$ | $d_{33}$ | $d_{12}$ | $q^2/q_0^2$ |
|---|---|---|---|---|---|---|---|---|---|---|
| 1D-2C | $k_1\neq 0$ | 0 | 0 | 1 | 0 | 0 | 1 | 0 | 0 | 1/2 |
| | $k_2\neq 0$ | 1/2 | 0 | 1/2 | 0 | 0 | 1 | 0 | 0 | 1 |
| | $k_3\neq 0$ | $(\eta-1)/(2\eta-1)$ | $\eta/(2\eta-1)$ | 0 | 0 | 0 | 0 | 1 | 0 | $(4B-1)/4B$ |
| 2D-3C | $k_3=0$ | 1/4 | 1/4 | 1/2 | 0 | 1/4 | 3/4 | 0 | 0 | 1 |
| | $k_1=0$ | $(\eta-1)/(2\eta-1)$ | $\eta/(4\eta-2)$ | $\eta/(4\eta-2)$ | 0 | 0 | 1/2 | 1/2 | 0 | $(4B-1)/4B$ |
| | $k_2=0$ | 0 | 0 | 1 | 0 | 0 | 1 | 0 | 0 | 0 |
| 3D-3C isotropic | | 0 | 0 | 1 | 0 | 0 | 1 | 0 | 0 | 0 |

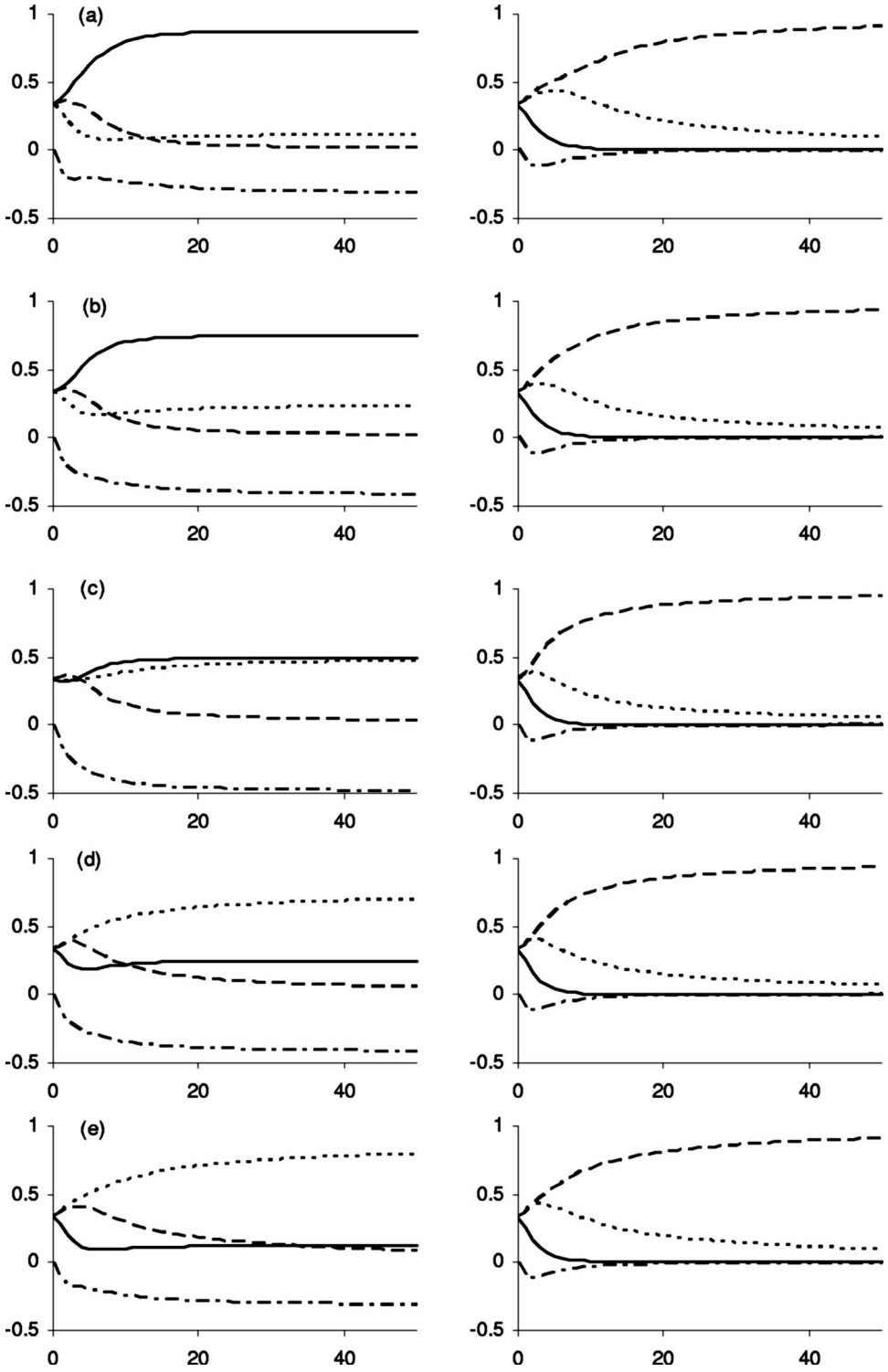


FIG. 4. Evolution of the normalized stresses (left) and the structure dimensionality (right) components: 11 (continuous), 22 (short-dashed), 33 (long-dashed), and 12 (dot-dashed) for $\eta = 0.125$ (a), 0.25 (b), 0.5 (c), 0.75 (d), and 0.875 (e), for an initially isotropic 3D turbulence.

$$\frac{R_{11}^{\mathrm{vor}}(\eta=1)}{q_0^2} = \frac{1}{2\sqrt{1+\beta^2}}, \quad \frac{R_{22}^{\mathrm{vor}}(\eta=1)}{q_0^2} = \frac{\beta^2}{2\sqrt{1+\beta^2}},$$
$$\frac{R_{33}^{\mathrm{vor}}(\eta=1)}{q_0^2} = \frac{1+\beta^2}{2\sqrt{1+\beta^2}}, \quad \frac{R_{12}^{\mathrm{vor}}(\eta=1)}{q_0^2} = -\frac{\beta}{2\sqrt{1+\beta^2}}. \tag{4.36}$$

The structure dimensionality tensor components are found to be equal to the respective stress components at any time

$$D_{ij}^{\mathrm{vor}}(\eta=1,\beta) = R_{ij}^{\mathrm{vor}}(\eta=1,\beta). \tag{4.37}$$

Such an equality has also been noted by Akylas *et al.*[21] for the analytical solution of the 3D initially isotropic case as well. Another similarity with the initially isotropic 3D solution is the linear evolution of the turbulent kinetic energy. None of the previously examined 1D or 2D initialized solutions matches this linearity. From (4.36) and (4.37), we may

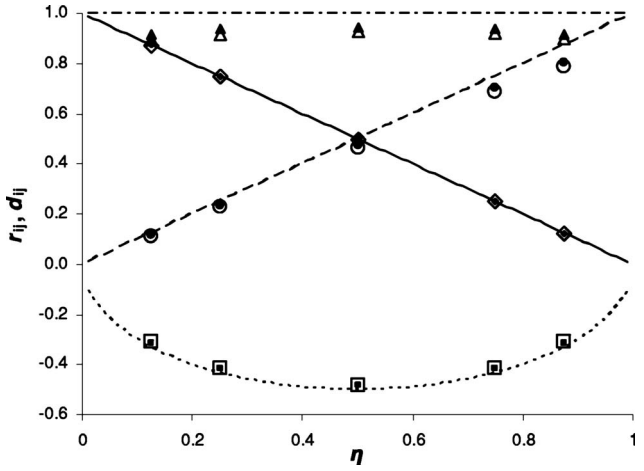


FIG. 5. Asymptotic values of the normalized stresses 11 (—; ◇; ♦), 22 (- - -; ○; ●), 12 (- - - -; □; ■) and the structure dimensionality component 33 (- · -; △; ▲) calculated analytically for the case with $k_1=0$ (lines) and at $\beta=50$, for the initially isotropic 3D case (solid symbols) and the 2D initialization with $k_2=0$ (open symbols).

note that the vortical solution starts as 2D-2C, evolves as 3D-3C and it is driven, asymptotically, to a 2D-2C final state with $r_{22}=d_{22}\rightarrow 0.5$, $r_{33}=d_{33}\rightarrow 0.5$, forming vortical axisymmetric eddies aligned with the axis of the mean flow $(x_1)$.

For the choice of a jetal initial turbulence, the integration of the spectral solution (4.35) yields

$$R_{11}^{\mathrm{jet}}(\eta=1)=\left[2+\frac{1}{(1+\beta^2)^{3/2}}-\frac{3}{\sqrt{1+\beta^2}}\right]\frac{q_0^2}{2\beta^2},$$

$$R_{22}^{\mathrm{jet}}(\eta=1)=\frac{2+\beta^2}{2(1+\beta^2)^{3/2}}q_0^2,$$

$$R_{33}^{\mathrm{jet}}(\eta=1)=\frac{2+\beta^2-2\sqrt{1+\beta^2}}{2\beta^2\sqrt{1+\beta^2}}q_0^2, \tag{4.38}$$

$$R_{12}^{\mathrm{jet}}(\eta=1)=\frac{\beta}{2(1+\beta^2)^{3/2}}q_0^2.$$

As a result, the 3C solution, obtained through the superposition of the vortical and the jetal cases, is dominated by the vortical solution.

On the other hand, at the transitional limit with $\eta=0$, the solution is driven by the jetal initialization, since the vortical initialization does not produce any stress evolution. In this jetal case, by taking the limit of $E_{12}(\eta=0)$ in Eqs. (4.35) and integrating over $\theta$, the shear stress becomes

$$\frac{R_{12}^{jet}(\eta=0)}{q_0^2}=\frac{\beta}{2(\beta^2+1)^{3/2}}-\frac{1}{2\pi}\int_0^{2\pi}\frac{\sin^2\theta/\cos\theta}{1+\beta^2\cos^2\theta}\arctan(\beta\cos\theta)d\theta, \tag{4.39}$$

where the evolution of $R_{12}^{\mathrm{jet}}(\eta=0)$ for large $\beta$ is determined by the value of the integral at the right-hand side of (4.39). Indeed, for large values of $\beta$, the limit of this integral is

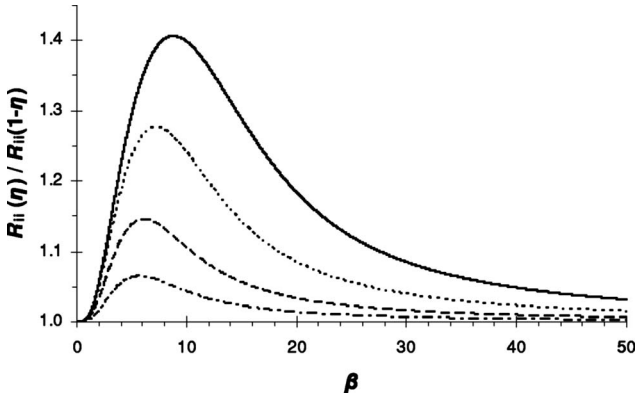


FIG. 6. Evolution of the turbulent kinetic energy ratio $R_{ii}(\eta)/R_{ii}(1-\eta)$, derived from the 3D-PRM numerical calculations for $\eta=0.0675$ (—), 0.125 (- - -), 0.25 (- -), and 0.375 (-·-).

$$R_{12}^{\mathrm{jet}}(\eta=0,\beta\gg)\rightarrow-\frac{2}{\pi}\int_0^{\infty}\frac{\arctan(\theta)}{x(1+\theta^2)}d\theta=-\ln 2, \tag{4.40}$$

which equals the respective asymptotic value estimated by Rogers[20] for the initially isotropic 3D case.

## V. COMPARISONS BETWEEN THE VARIOUS NONISOTROPIC INITIALIZATIONS AND THE 3D INITIALLY ISOTROPIC CASE

As shown in the analysis presented in Sec. IV, three out of the six alternative nonisotropic initializations that have been examined for the solution of the system (2.6), resulted in a dependence on the dimensionless rotation rate $\eta$; the 1D-2C initialization with $k_3\neq 0$, the 2D-3C with $k_1=0$ and the 2D-3C initialization with $k_2=0$. Clearly, for all the above solutions the dependence on the axis of the frame rotation $x_3$ (meaning that $k_3\neq 0$) is present. The other $(k_3=0)$ is the material indifferent case. Due to profound qualitative similarities between the behavior of the first two choices (1D with $k_3\neq 0$, 2D with $k_1=0$) as discussed, in this section we focus on the comparison of only the last two 2D-3C initializations $(k_1=0, k_2=0)$ with the initially isotropic 3D-3C solution. For the case with $k_1=0$, the calculations of the one-point statistics have been done analytically through the respective relations derived in Sec. IV B 2, while when $k_2=0$, we use the numerical integrations of the relevant spectral solutions derived in Sec. IV B 3. Finally, the results for the initially isotropic 3D initialization have been calculated through the PRM (Kassinos and Reynolds[23]) exact numerical solution. The comparisons refer to the dimensionless stresses $r_{ij}$, structure dimensionality tensor components $d_{ij}$, and the evolution of the turbulent kinetic energy $q^2/2$, and they are presented for the following ranges of the values of $\eta$:

- $0<\eta<1$, which determines the unstable regime where the energy grows exponentially with time,
- $\eta=0$ and $\eta=1$, the transitional regime where the energy growth shifts from exponential to algebraic, and
- $\eta>1$ and $\eta<0$, the stable regime, where the energy stabilizes.

The asymptotic limits for large total shear of all the compared parameters are summarized in Tables I–IV.

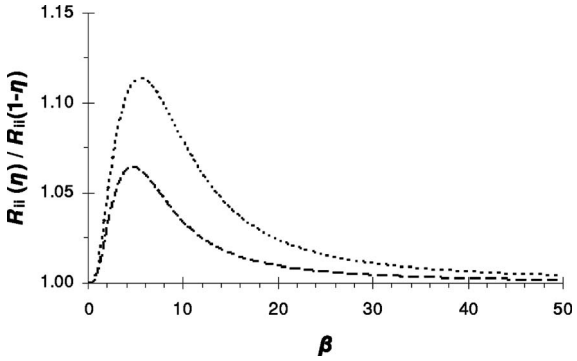


FIG. 7. Evolution of the turbulent kinetic energy ratio $R_{ii}(\eta)/R_{ii}(1-\eta)$, for the initialization with $k_2=0$, calculated with superposition between equally divided vortical and jetal initial spectra for $\eta=0.125$ (short-dashed) and 0.25 (long-dashed).

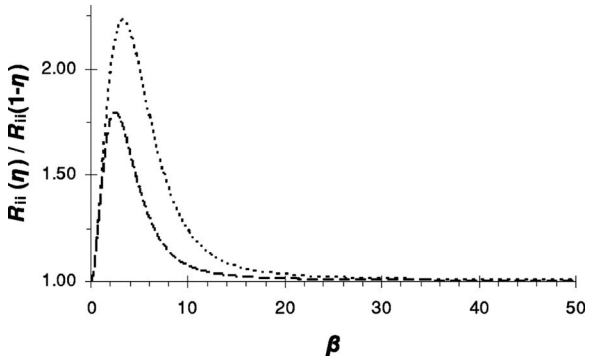


FIG. 9. As in Fig. 6, but with $R_{ii}(\eta)$ for a jetal initialization and $R_{ii}(1-\eta)$ for a vortical initialization.

### A. Unstable regime

From the investigation of the 3D PRM results, we observe (Fig. 4) that, in all cases characterized by a positive Bradshaw number[19,29] $B=\eta(1-\eta)$, meaning $0<\eta<1$, the 3D-3C initially isotropic turbulence is driven quite fast to the 1D-2C asymptotic state: $d_{33}\to 1$, $r_{33}\to 0$. The above finite 1D asymptotic behavior makes it possible to represent this regime quite accurately, using the simplified fully 2D analysis of the problem with the $k_1=0$ state (independent of $x_1$). Indeed, for values of $\eta$ between 0 and 1, the qualitative agreement between the analytical results of this specific 2D approach and the 3D-3C exact PRM numerical solutions is in general accurate. More specifically, in terms of the normalized stresses and the structure dimensionality components, the 2D analytical solution derived in Sec. IV B 2 and the 3D PRM exact numerical solution collapse quickly to the same asymptotic state [Eqs. (4.25) and (4.26)]. The asymptotic limits for the 2D case with $k_1=0$ can be calculated analytically through Eqs. (4.25) and (4.26), for vortical and jetal initializations, respectively. The results for both initializations are identical and are summarized in Table I. As shown in Fig. 5, the same limits are also reached by both the 3D isotropic case (initially) and the 2D initialization with $k_2=0$.

In this unstable regime, the energy $R_{ii}$ evolves exponentially with time, growing faster as $\eta$ approaches 0.5 (Brethouwer[4]). The solutions for the isotropic 3D initialization showed that the evolution histories for small total shear, depend not only on $B=\eta(1-\eta)$ but also on $\eta$. That is, we obtain different histories between cases with identical $B=\eta(1-\eta)$ and different $\eta$ (pointed out also by Salhi[19]), with $R_{ii}(\eta,\beta)$ being larger than $R_{ii}(1-\eta,\beta)$ for $0<\eta<0.5$. However, we found that there exists a clear trend for a matching asymptotic behavior; i.e., $R_{ii}(1-\eta,\beta\gg 1)\to R_{ii}(\eta,\beta\gg 1)$, as shown in Fig. 6. From the investigation of the numerical solution of the initially 2D case, with $k_2=0$, we can show that there exists a similar matching asymptotic behavior in the evolution of $R_{ii}(\eta,\beta)$ and $R_{ii}(1-\eta,\beta)$, only when a superposition with equally weighted (50%-50%) vortical and jetal initializations is used (Fig. 7). This behavior is attributed to the fact that, besides strong deviations at early times, the vortical part of the solution for $R_{ii}(\eta,\beta)$ matches gradually the jetal part of the solution for $R_{ii}(1-\eta,\beta)$, and vice versa; the jetal part of the solution for $R_{ii}(\eta,\beta)$ matches gradually the vortical part of the solution for $R_{ii}(1-\eta,\beta)$ as shown in Figs. 8 and 9, respectively. Even more, from the 2D approach with $k_1=0$ it is shown in Eqs. (4.16) and (4.19) that the vortical/jetal part of the solution for $R_{ii}(\eta,\beta)$ exactly matches the jetal/vortical part of the solution for $R_{ii}(1-\eta,\beta)$ at any time. As a result, a superposition weighted

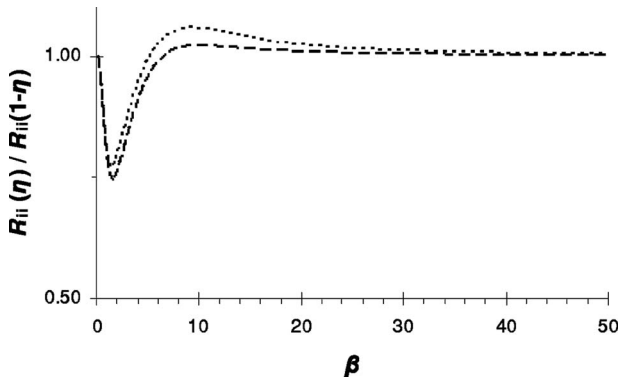


FIG. 8. Evolution of the turbulent kinetic energy ratio of $R_{ii}(\eta)$ for a vortical initialization divided by $R_{ii}(1-\eta)$ from a jetal initialization, calculated from the initially 2D case with $k_2=0$, for $\eta=0.125$ (short-dashed) and 0.25 (long-dashed).

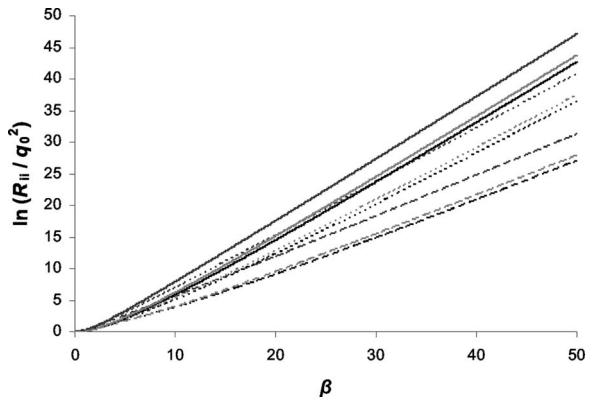


FIG. 10. Energy growth for $\eta=0.125$ (long-dashed), 0.25 (short-dashed), and 0.5 (continuous) for the 3D isotropic (black), the 2D initializations with $k_2=0$ (light gray) and $k_1=0$ (dark gray).

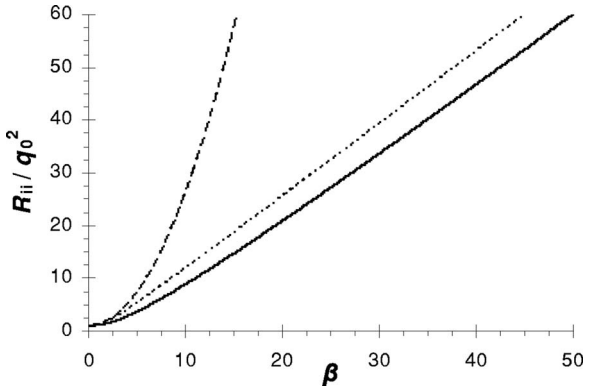


FIG. 11. Turbulent kinetic energy growth for $\eta=0$ and for 3D isotropic (solid) and 2D initializations with $k_2=0$ (only the jetal part of the solution) (short-dashed) and $k_1=0$ (long-dashed).

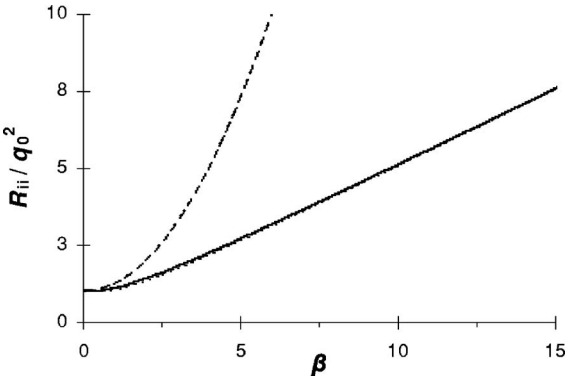


FIG. 12. As in Fig. 11, but for $\eta=1$, and using a 50%-50% superposition for both the 2D initializations.

again equally between the 2D jetal and vortical initializations, results in exactly the same turbulent kinetic energy growth, for cases characterized by the same $B$. In this case, the energy growth in the 2D approach for $k_1=0$, is calculated analytically by combining Eqs. (4.16) and (4.19) as

$$\frac{R_{nn}(\beta,k_1=0)}{q_0^2}=\frac{I_0[2\sqrt{\eta(1-\eta)}\beta]-(2\eta-1)^2}{4\eta(1-\eta)}, \tag{5.1}$$

and reaches the following asymptotic form at large values of total shear

$$\frac{R_{nn}(\beta\gg 1,k_1=0)}{q_0^2}\rightarrow\frac{\exp(2\beta B^{1/2})}{8\sqrt{\pi}\beta^{1/2}B^{5/4}}, \tag{5.2}$$

depending only on the Bradshaw number $B=\eta(1-\eta)$ and $\beta$. Using a simplified 3D analysis, neglecting the pressure strain-correlations, Brethouwer[4] derived the dominating exponential energy growth $\sim\exp(2\beta B^{1/2})$. As noticed earlier in this study, the same exponential asymptotic behavior is found even if we work out the 1D solution for $k_1=k_2=0$ (Sec. IV A 1).

In Fig. 10 we present a comparison, in terms of the energy growth, between the three different initializations examined. From this figure it is apparent that, as already noticed, for any of the presented initializations, the rate of the energy growth increases as $\eta$ approaches 0.5, which results in the maximization of the exponential term $\exp(2\beta B^{1/2})$. However, we may notice the inequality between the turbulent kinetic energy calculated from the three different initializations: $R_{ii}(\eta,\beta,k_1=0)>R_{ii}(\eta,\beta,k_2=0)>R_{ii}(\eta,\beta,3\mathrm{D})$. This inequality is consistent with the following estimates of the asymptotic turbulent kinetic energy growth in the last two initializations.

In the case of $k_2=0$, the investigation of the spectral solution showed that

$$\frac{R_{nn}(\beta\gg 1,k_2=0)}{q_0^2}\rightarrow\frac{\exp(2\beta B^{1/2})}{C_1\beta^{3/2}B^{5/4}}, \tag{5.3}$$

with $C_1\approx 8.1$. For the initially isotropic 3D turbulence we have concluded, using the numerical results, that the finite asymptotic state of the energy evolution is reached at larger times ($\beta\sim 100$), when it becomes

$$\frac{R_{nn}(\beta\gg 1)}{q_0^2}\rightarrow\frac{\exp(2\beta B^{1/2})}{C_2\beta^2B^{3/2}}, \tag{5.4}$$

with $C_2\approx 4.6$.

### B. Transitional regime

The transitional regime is characterized by $B=0$, which means that $\eta$ is either 0 (no rotation) or 1 (counter-rotating frame). As mentioned, these two cases have been studied analytically for an initially isotropic 3D state, by Rogers[20] and Akylas *et al.*,[21] respectively. Starting from the 2D initialization with $k_1=0$, we show that it drives turbulence to a different asymptotic behavior compared to the 3D isotropic case. The main difference lies into the different estimation of the energy growth as $R_{nn}(\beta)=O(\beta^2)$, which does not agree with the linear behavior of the 3D initially isotropic solution,

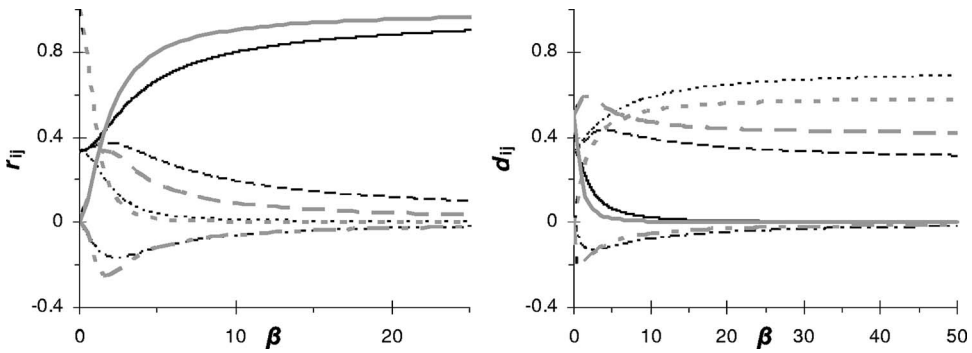


FIG. 13. Evolution of the normalized stress and the normalized structure dimensionality components 11 (continuous), 22 (short-dashed), 33 (long-dashed), and 12 (dot-dashed) for $\eta=0$ and for the 3D isotropic initialization (thin black) and the 2D initialization with $k_2=0$ (only the jetal part of the solution) (bold gray).

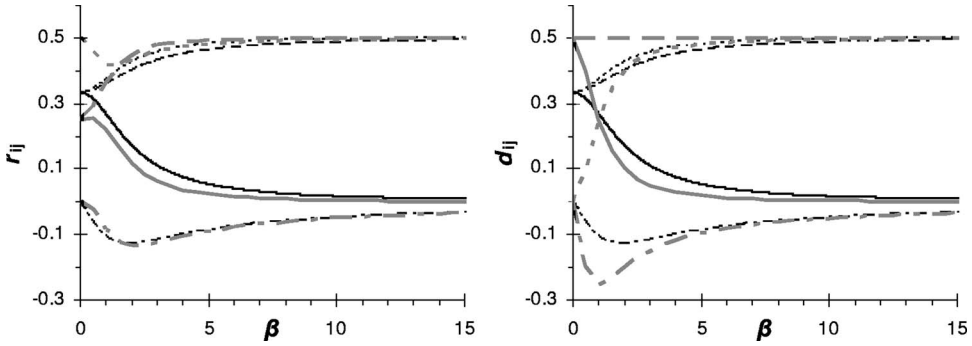


FIG. 14. As in Fig. 13, but for $\eta=1$.

as shown in Figs. 11 and 12. Also the asymptotic states for the normalized stresses and structure dimensionality tensor components [Eqs. (4.22) and (4.24)], summarized in Tables II and III, do not match those from the 3D solution (with the only exception being the asymptotic state for the normalized stress component $r_{11}\rightarrow 1$, for $\eta=0$).

In contrast to the $k_1=0$ initialization, when $k_2=0$ the calculations are highly comparable with the results of the initially isotropic 3D case, in terms of the turbulent kinetic energy (Figs. 11 and 12) and the normalized stresses and structure dimensionality components (Figs. 13 and 14). Especially for $\eta=1$, there is an impressive agreement between the two solutions. They both converge to the same vortical 2D-2C axisymmetric asymptotic state with $d_{11}=r_{11}\rightarrow 0$, $d_{22}=r_{22}\rightarrow 1/2$ and $d_{33}=r_{33}\rightarrow 1/2$. The fact that this state is reached relatively quickly ($\beta\approx 5$) would seem to suggest that the simplified analysis with $k_1=0$ would provide a good approximation to the exact evolution of the tensor components. However, as noted previously, such an approximation fails to capture the correct turbulent kinetic energy growth, suggesting that for the transitional cases the 3D character of the turbulence at early times plays a key role in determining the evolution at later times (this also holds true for the case without any frame rotation).

### C. Stable regime

The stable cases are characterized by $B<0$ (either $\eta<0$ or $\eta>1$). Figures 15 show that for negative values of $\eta$, the 3D-3C calculations for the evolution of the turbulent kinetic energy lie between the respective ones from the 2D cases, with $k_1=0$ (larger) and with $k_2=0$ (smaller). More specifically, as shown analytically in Sec. IV B 2, when $k_1=0$ the energy level approaches a fixed state with decreasing oscillations with a period proportional to $2\sqrt{-B}$ [Eqs. (4.16) and (4.19)]. This solution fails to capture the clear diminishing behavior of the kinetic energy found with the 3D isotropic initialization. On the other hand, when $k_2=0$ the energy diminishes, although remaining smaller compared to the fully 3D case. This difference can be attributed to the clear increase of the energy at short times, which exists in the initially isotropic case, but it is not as intense for the $k_2=0$ initialization. The last remark is due mainly to the fact that in this study we have used a uniform 50%-50% superposition between the jetal and the vortical part for the 2D solution. For $\eta<0$, the jetal part of this specific 2D solution shows a significant initial increase in the turbulent kinetic energy, while the vortical part decreases monotonically (not shown here). As a result, different choices for the weights of the

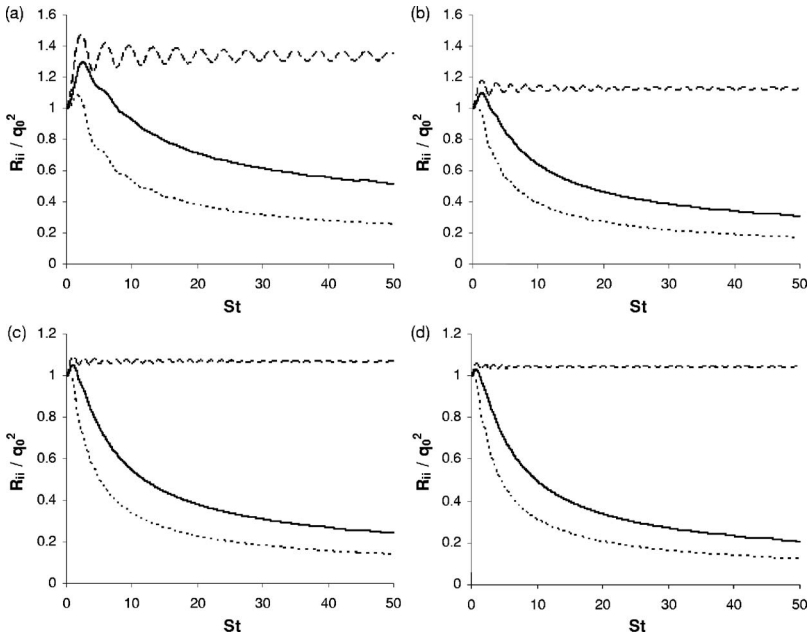


FIG. 15. Evolution of the turbulent kinetic energy for the stable cases with $\eta=-0.5$ (a), $-1.0$ (b), $-1.5$ (c), and $-2.0$ (d). The curves correspond to three different initial states examined: (continuous) isotropic 3D-3C, (long-dashed) 2D-3C with $k_1=0$ and (short-dashed) 2D-3C with $k_2=0$. In the 2D (initially) cases, a superposition of equally weighted vortical and jetal initializations has been used.

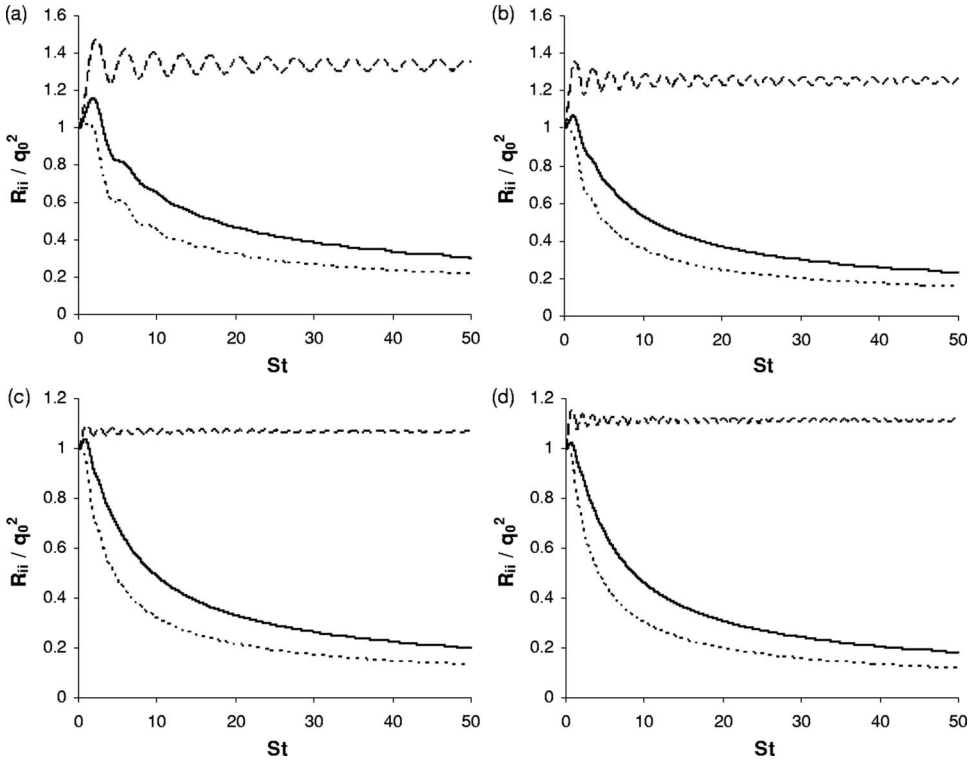


FIG. 16. As in Fig. 15, but for the stable cases with $\eta=1.5$ (a), 2.0 (b), 2.5 (c) and 3.0 (d).

superposition (dependent, however, on the value of $\eta$) can improve this feature. However, the investigation of this feature is beyond the general scope of this study and here we use an equally divided partition. In any case, the deviation between the 2D initialization and the 3D isotropic solution seems to shrink, in general, as the stability is enhanced (the absolute value of $\eta$ is increased). Similar results can be drawn also for the cases with positive $\eta$ (Fig. 16), with the only exception that for this direction of the frame rotation the initial increase of the energy is due to the vortical part of the solution.

Focusing in the 3D initialization, we may notice (Fig. 17) that the cases with $\eta>1$ result in a lower energy compared to the cases with $\eta<0$, for the same value of $B$. This difference exhibits a decreasing trend as the stability is increased. A similar picture can be drawn also for the results of

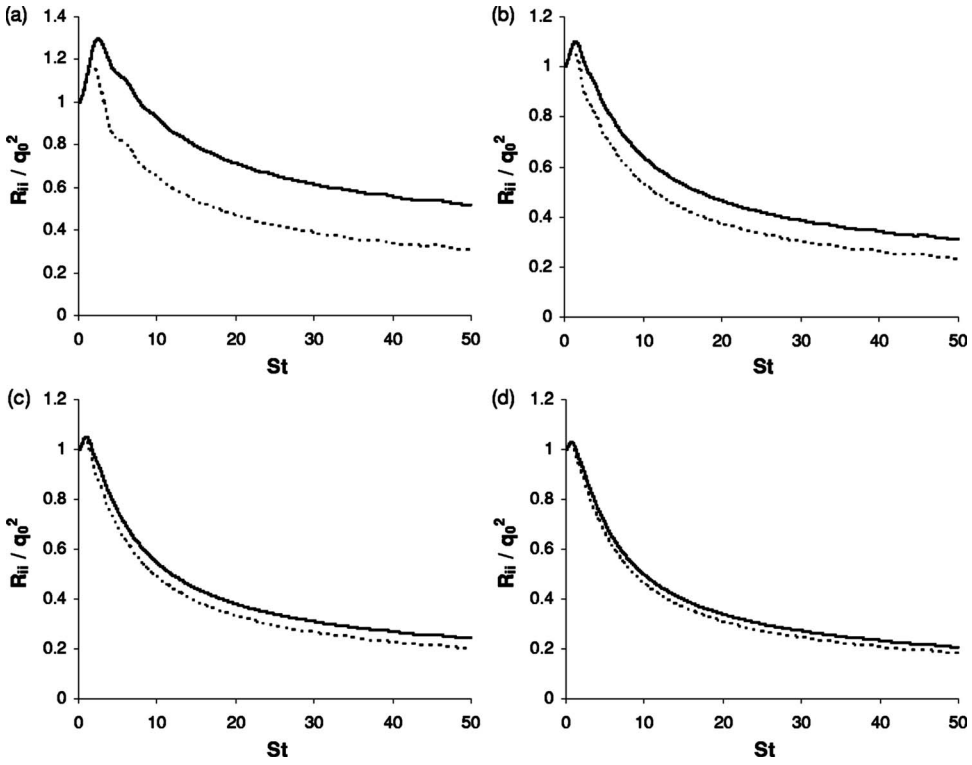


FIG. 17. Comparisons of the evolution of the turbulent kinetic energy starting with an isotropic 3D-3C state, for stable cases with the same $B$ and for $\eta=1.5/-0.5$ (a), $2.0/-1.0$ (b), $2.5/-1.5$ (c), and $3.0/-2.0$ (d). The continuous curves correspond to negative values of $\eta$ and the dashed lines to positive.

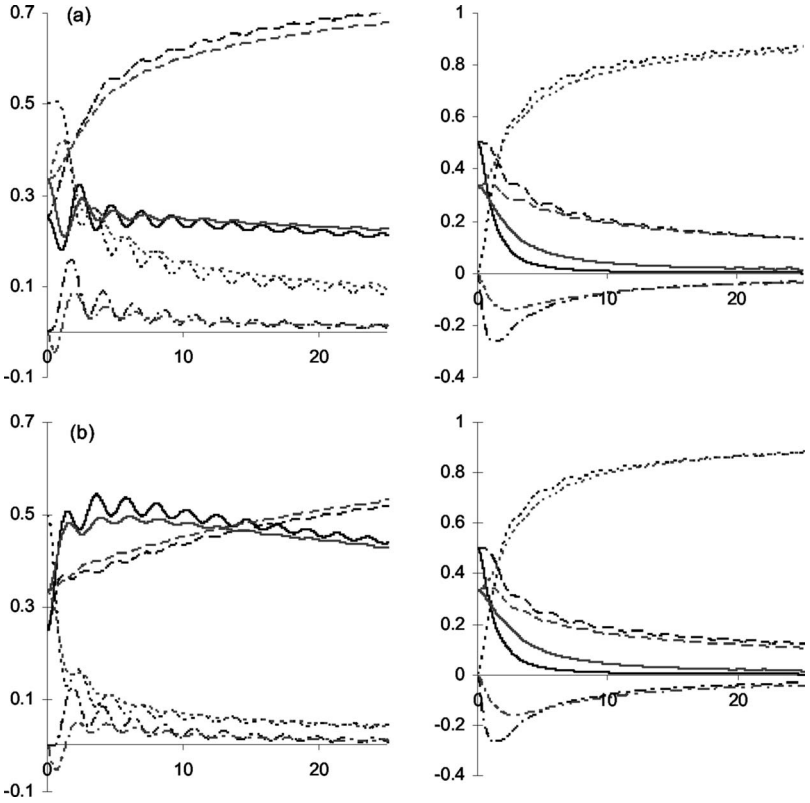


FIG. 18. Evolution of the normalized stresses (left) and the structure dimensionality (right) components: 11 (continuous), 22 (short-dashed), 33 (long-dashed), and 12 (dotted dashed) for $\eta=2.0$ (a) and $-1.0$ (b). The black lines correspond to the solution for $k_2=0$ and the gray lines to the PRM exact numerical solution for an initially isotropic 3D condition.

the solution with $k_2=0$ (not shown here). In contrast to the above mentioned asymmetry, when $k_1=0$ the cases being characterized by an equal $B$ show exactly the same energy evolution for a 50%-50% superposition between the vortical and the jetal part of this specific solution. This can be explained by the fact that for this particular initialization, the vortical/jetal part of the solution for $R_{ii}(\eta,\beta)$ equals the jetal/vortical part of the solution for $R_{ii}(1-\eta,\beta)$ at any time, as shown in the respective Eqs. (4.16) and (4.19).

From the above discussion, it follows that the results of the 2D initialization with $k_2=0$ (which generates a 3D state) are as close as possible to the ones from the 3D isotropic initialization. This may also be concluded by the agreement in the evolutions of the dimensionless stress and structure dimensionality components as shown in Fig. 18. From the same figure it becomes clear that for the stable cases the turbulence keeps a 3C-3D character for much longer times compared to the unstable cases. Thus, it is not surprising that for the stable regime the initial dependence on the axis of the mean flow, i.e., $x_1$, is also important (along with the dependence on the axis of the frame rotation, i.e., $x_3$) for the evolution of the turbulence with time. The final state for the stable cases is approached at very large times, with the turbulence evolving very slowly towards an 1D-1C with $r_{33}\rightarrow 1$, $d_{22}\rightarrow 1$. That is, formation of sheets perpendicular to the axis of the mean gradient with turbulent velocity fluctuations around the axis of the frame rotation. However, at those large times, the turbulent kinetic energy almost vanishes.

## VI. CONCLUSIONS

In this study we examined the effect of the initial conditions of the turbulence for rapidly distorted shear flow in a rotating frame. Analytical solutions have been derived for the evolution of the Reynolds stresses and the structure dimensionality tensor components for three one-dimensional and three two-dimensional initializations. Consistent with the material indifference of 2D turbulence, we found that when the turbulence is initially independent on the axis of the frame rotation ($k_3=0$), the solutions are not sensitive to the dimensionless rotation rate $\eta$. In the more important general case with $k_3\neq 0$, the solutions are separated in four classes, according to the value of $\eta$, with three corresponding energy evolution regimes: unstable, stable, or transitional.

In the unstable regime, the solutions exhibit a similar asymptotic behavior in terms of the evolution of the normalized stresses and the structure dimensionality components, approaching quickly a 2C-1D final state, with all the spatial dependence being on the axis of the frame rotation. The turbulent kinetic energy grows exponentially with time for all cases, although clearly faster when $k_1=0$. When $k_2=0$, the calculated energy growth was found to be much closer to the initially isotropic 3D case. Small deviations, in the energy growth, between cases characterized by a different dimensionless rotation ratio $\eta$, but the same parameter $B=\eta(1-\eta)$, were noticed for both the fully 3D and the initially 2D (with $k_2=0$) solutions, while they were absent when $k_1=0$. However, the relative deviations decrease with time and the asymptotic states, for large total shear, depend only on the value of parameter $B$. In the transitional regime the 2D initialization with $k_1=0$ drives turbulence to a completely different asymptotic behavior compared to the 3D isotropic case. The main difference lies into the different estimation of the energy growth, as $R_{nn}(\beta)\sim\beta^2$, which does not agree with the linear behavior of the 3D initially isotropic solution. In contrast to that, when the initial dependence on the axis of

the mean flow is present, i.e., $k_1 \neq 0$, $k_3 \neq 0$, and $k_2 = 0$, the calculations are highly comparable with the results for the initially isotropic 3D case, in terms of both the turbulent kinetic energy evolution and the dimensionless stress and structure dimensionality components.

For the stable regime it has been shown that the 3D-3C character of the turbulence at early times is crucial for the evolution of the kinetic energy, unlike in the unstable cases. The initializations with $k_1 = 0$ deviate from the initially isotropic case, failing to capture the decay of the turbulent kinetic energy at large times. On the other hand, both the 3D isotropic and the 2D initialization with $k_2 = 0$, which migrates to 3D, cause a diminishing behavior of turbulent kinetic energy (TKE) at large enough times. The similarity of the last two solutions in terms of the normalized stresses and the structure dimensionality components is remarkable.

## ACKNOWLEDGMENTS

This work has been performed under the UCY-CompSci project, a Marie Curie Transfer of Knowledge (TOK-DEV) grant (Contract No. MTKD-CT-2004-014199), and under the SBM-EuroFlows project, a Marie Curie IRG grant (Contract No. MIRG-CT-2004-511097) both funded by the CEC under the 6th Framework Program.

[1] J. Bardina, J. H. Ferziger, and W. C. Reynolds, "Improved turbulence models based on large-eddy simulation of homogeneous incompressible turbulent flows," Tech. Rep. TF-19, Department of Mechanical Engineering, Stanford University, Stanford, CA, 1983.
[2] J. M. Lee, J. Kim, and P. Moin, "Structure of turbulence at high shear rate," J. Fluid Mech. **216**, 561 (1990).
[3] A. Salhi and C. Cambon, "An analysis of rotating shear flow using linear theory and DNS and LES results," J. Fluid Mech. **347**, 171 (1997).
[4] G. Brethouwer, "The effect of rotation on rapidly sheared homogeneous turbulence and passive scalar transport. Linear theory and direct numerical simulation," J. Fluid Mech. **542**, 305 (2005).
[5] S. B. Pope, *Turbulent Flows* (Cambridge University Press, Cambridge, 2000), p. 421.
[6] H. Hanazaki and J. C. R. Hunt, "The structure of unsteady stably stratified turbulence with mean shear," J. Fluid Mech. **507**, 1 (2004).
[7] S. C. Kassinos and W. C. Reynolds, "A structure based model for the rapid distortion of homogeneous turbulence," Tech. Rep. TF-61, Department of Mechanical Engineering, Stanford University, Stanford, CA, 1994.
[8] P. R. Spalart, "Direct simulation of a turbulent boundary layer up to $R_\theta = 1410$," J. Fluid Mech. **187**, 61 (1988).
[9] R. D. Moser, J. Kim, and N. N. Mansour, "Direct numerical simulation of turbulent channel flow up to $\mathrm{Re}_\tau = 590$," Phys. Fluids **11**, 943 (1999).
[10] R. E. Britter, J. C. R. Hunt, and K. J. Richards, "Air flow over a two-dimensional hill: studies of velocity speedup, roughness effect and turbulence," J. Quant. Spectrosc. Radiat. Transf. **107**, 91 (1981).
[11] W. Gong, P. A. Taylor, and A. Dombrack, "Turbulent boundary-layer flow over fixed aero-dynamically rough two-dimensional sinusoidal waves," J. Fluid Mech. **312**, 1 (1996).
[12] M. Galmiche and J. C. R Hunt, "The formation of shear and density layers in stably stratified turbulent flows: linear processes," J. Fluid Mech. **455**, 243 (2002).
[13] S. Nazarenko, "Exact solutions for near-wall turbulence theory," Phys. Lett. A **264**, 444 (2000).
[14] A. A. Townsend, *The Structure of Turbulent Shear Flow*, 2nd ed. (Cambridge University Press, Cambridge, 1976).
[15] J. C. R. Hunt, "A review of the theory of rapidly distorted turbulent flow and its applications," Fluid Dyn. Trans. **9**, 121 (1978).
[16] A. M. Savill, "Recent developments in rapid distortion theory," Annu. Rev. Fluid Mech. **19**, 531 (1987).
[17] J. C. R. Hunt and D. J. Carruthers, "Rapid distortion theory and the 'problems' of turbulence," J. Fluid Mech. **212**, 497 (1990).
[18] C. Cambon and J. F. Scott, "Linear and nonlinear models of anisotropic turbulence," Annu. Rev. Fluid Mech. **31**, 1 (1999).
[19] A. Salhi, "Similarities between rotation and stratification effects on homogeneous shear flow," Theor. Comput. Fluid Dyn. **15**, 339 (2002).
[20] M. M. Rogers, "The structure of a passive scalar field with a uniform mean gradient in rapidly sheared homogeneous turbulent flow," Phys. Fluids A **3**, 144 (1991).
[21] E. Akylas, S. C. Kassinos, and C. A. Langer, "Analytical solution for a special case of rapidly distorted turbulent flow in a rotating frame," Phys. Fluids **18**, 085104 (2006).
[22] S. C. Kassinos, W. C. Reynolds, and M. M. Rogers, "One-point turbulence structure tensors," J. Fluid Mech. **428**, 213 (2001).
[23] S. C. Kassinos and W. C. Reynolds, "A particle representation model for the deformation of homogeneous turbulence," in *Annual Research Briefs 1996* (Stanford University and NASA Ames Research Center: Center for Turbulence Research, Stanford, CA, 1996), pp. 31–50.
[24] S. C. Kassinos, C. A. Langer, G. Kalitzin, and G. Iaccarino, "A simplified structure-based model using standard turbulence scale equations: computation of rotating wall-bounded flows," Int. J. Heat Fluid Flow **27**, 653 (2006).
[25] R. S. Rogallo, "Numerical experiments in homogeneous turbulence," NASA Tech. Memo 81315 (1981).
[26] W. C. Reynolds, "Effects of rotation on homogeneous turbulence," in Proceedings of the 10th Australasian Fluid Mechanics Conference, University of Melbourne: Melbourne, Australia, 1989.
[27] S. C. Kassinos, B. Knaepen, and D. Carati, "The transport of a passive scalar in magnetohydrodynamic turbulence subjected to mean shear and frame rotation," Phys. Fluids **19**, 015106 (2007).
[28] C. G. Speziale, "Some interesting properties of two-dimensional turbulence," Phys. Fluids **24**, 1425 (1981).
[29] P. Bradshaw, "The analogy between streamline curvature and buoyancy in turbulent shear flow," J. Fluid Mech. **36**, 177 (1969).